Influence of Stiffness, Monomer Structure, and Energetic Asymmetries on Polymer Blend Miscibilities: Applications to Polyolefins

K. W. Foreman and Karl F. Freed*

The James Franck Institute and the Department of Chemistry, University of Chicago, Chicago, Illinois 60637

Received March 11, 1997; Revised Manuscript Received September 2, 1997[⊗]

ABSTRACT: The generalization of the lattice cluster theory (LCT) to include explicit trans−gauche energy differences is applied to study the combined influences of chain stiffness disparities, monomer molecular structures, energetic asymmetries, and nonrandom mixing on the miscibilities of binary polymer blends. The combination of all these relevant physical features within a single theory enables testing various divergent suggestions concerning the dominant physical factors governing the miscibility of polyolefin blends. Thus, tests are presented of models ascribing the observed miscibility patterns in polyolefin blends solely to entropic factors (stiffness disparities) or solely to enthalpic factors (solubility parameter models). The LCT computations demonstrate the combined importance of both factors, as well as several others arising from monomer molecular structures and compressibility. An important and highly nontrivial ingredient in these tests is the novel computation of the mean square radius of gyration for structured monomer chains. The LCT also provides partial tests of a model in which thermodynamically equivalent semiflexible linear chains replace real polyolefin chains. In addition, we extend to semiflexible chains and to asymmetric polymerization indices a remarkable correlation between the binary blend critical temperature and a structural parameter that depends on the fractions of tri- and tetrafunctional united atom groups in the component chains (for model blends in which all van der Waals interactions are equal). Several comparisons with experiment for polyolefin blends serve to explain the molecular origins of observed deviations from solubility parameter models for the phase behavior of blends containing poly(isobutylene), as well as for the observed very weak variation of the critical temperature with molecular weights observed in some experimental blends.

I. Introduction

The preparation of polymer blends with controlled properties poses enormous scientific and technological challenges. This endeavor is becoming feasible, however, for polyolefin blends where metallocene catalysts allow the tailoring of polyolefins on the molecular level. Thus, progress in fabricating polyolefin systems with desired properties requires knowledge of the relation between the molecular level details of the controlled syntheses and the specific physical properties of the final composite material. Another example of the great interest in developing controlled polymer blends involves producing miscible blends whose constituents are the generally immiscible rigid and flexible polymers.[1] The resulting blend is expected to be similar to a composite material but is rigid enough to resist deformation on a molecular level, while the flexible component imparts elasticity to the material. In general, the success in generating polyolefin blends or rigid−flexible polymer blends rests in accurately relating the phase behavior of the desired systems to the molecular structures and mutual interactions of the constituents.

Recent experiments by Lohse, Graessley and co-workers[2−7] find that most polyolefin blend miscibilities roughly correlate with the solubility parameters either determined from small-angle neutron scattering or deduced from equation of state data for the pure components. These findings suggest that the polyolefin miscibility patterns are determined mostly by the slight energetic differences between the two blend components. Several blends, however, deviate strongly from this simple model, especially those containing poly(isobutylene) (PIB), and all exhibit lower critical solution temperature (LCST) phase diagrams. The explanation of the deviations from a solubility parameter model generally requires a deeper understanding based on a more microscopic investigation of the factors affecting blend miscibilities, and several theories have been proposed to deal with various aspects of this problem.

Bates, Fredrickson, and co-workers [8−12] have introduced a simple alternative model (the BF model) for polyolefin miscibilities. The BF model appends Gaussian fluctuations to incompressible Flory−Huggins (FH) theory, and the only important parameter influencing polyolefin blend miscibility arises from the difference in chain stiffnesses for the two blend components. This model ascribes polyolefin miscibility patterns solely to *entropic* factors. Implicit in the BF model is the further prediction that an immiscible polyolefin blend may be transformed into a purely miscible one simply by modifying one component so that a stiffness parameter is identical for both components. The purely entropic BF model explains only a portion of the polyolefin data and cannot describe the observed LCST behavior of the PIB systems. Moreover, the fact that the polyolefin melts have different reduced temperatures and reduced pressures indicates the presence of energetic differences between the polyolefins, differences that correlate with the alternative solubility parameter models.

Schweizer and co-workers[13,14] apply the more molecularly oriented PRISM integral equation methods to an off-lattice model of linear hard sphere chains whose stiffness is adjusted by use of a bending energy parameter. The PRISM computations imply that constant volume "athermal" systems with no additional interactions (beyond hard spheres and bending energies) can indeed phase separate due to stiffness disparities, in accord with the prediction of the BF model. The computed critical polymerization indices N_c for phase

[⊗] Abstract published in *Advance ACS Abstracts,* November 1, 1997.

S0024-9297(97)00337-9 CCC: $14.00

separation, however, greatly exceed those required experimentally for polyolefin blends. The PRISM computations find that phase separation occurs more readily with "thermal" models in which the chains also interact with Lennard−Jones potentials. The general trends from the more realistic "thermal" models qualitatively accord with experiments for a wide class of blends. Schweizer and Kumar[15−17] design these hard-sphere chain "thermal" models to mimic realistic polymer melts by choosing the bending energy E_b of a linear chain such that the respective intra- and intermolecular melt pair correlation functions, the aspect ratios, and the packing fractions are all nearly identical for the experimental systems and for the semiflexible linear chains used to model them. The objective here is to simplify the numerical analysis by introducing a semiflexible linear chain model that, to a good approximation, is thermodynamically equivalent to the original chain.

We, therefore, show how the lattice cluster theory (LCT) may be used to provide partial tests of the thermodynamically equivalent chain model. A truly equivalent chain would be completerly miscible with the original chain, and LCT phase diagrams are readily computed for blends containing the branched chains and the approximate thermodynamically equivalent model chains. The numerical PRISM computations include entropic contributions, and the atomistic blend PRISM computations of Curro and co-workers[16b] also explicitly account for nonspherical monomer shape and side branches. However, the analytical PRISM computations do not readily include these contributions. Hence, the analytical LCT is appied here to assess directly all the *entropic* contributions possibly affecting the observed miscibility patterns in polyolefins.

Dudowicz and Freed[18,19] have already used the LCT to study the influence of local monomer structures on the miscibilities of polyolefin systems. The Dudowicz−Freed model employs monomers that extend over several lattice sites, as dictated by the united atom structures of those monomers. While excluded volume constraints impart to the chains some degree of stiffness, the extended lattice model of the LCT lacks an extra explicit bending energy necessary to specify a particular chain stiffness. Nevertheless, the LCT description contains a degree of local chain stiffness, nonrandom mixing, and noncombinatorial corrections to the entropy, features which represent a combination of molecular characteristics suggested to govern polyolefin miscibilities by the solubility parameter model, by the models used in PRISM calculations, or by the BF model. Initial LCT calculations by Dudowicz and Freed[19] choose all united atom CH_n ($n = 0-3$) groups to interact with the same attractive van der Waals energy ϵ in order to focus on the influence of short chain branching. The analogous Flory−Huggins model with identical interaction energies between all components predicts completely miscible systems. Dudowicz and Freed, in contrast, find a vast range of blend miscibilities that correlate strongly with a simple structural parameter r^2 which is a function of the fractions of tri- and tetrafunctional carbons in the polyolefin chains[18] (see below). The most interesting features of their LCT computations are the strong sensitivity of the critical temperatures T_c to the monomer structures and the linear correlation of T_c/M with the simple entropic structural parameter r^2, where M is the total number of united atom groups in a chain. Dudowicz and Freed demonstrate that this useful relationship is highly sensitive to disparities between the three van der Waals interactions, a sensitivity which mirrors the sensitivity of Flory−Huggins theory predictions to both the sign and magnitude of the exchange energy

$$\epsilon_{ex} = \epsilon_{11} + \epsilon_{22} - 2\epsilon_{12} \tag{1.1}$$

The additional dependence of the LCT free energy on differences $\epsilon_{ij} - \epsilon_{lm}$ reflects often ignored energetic consequences of blend compressibility. Prior discussions of compressibility generally focus on "equation of state effects" arising from differences in the melt specific volumes of the two components. Within structureless monomer models, asymmetric self-interaction energies $\epsilon_{11} \neq \epsilon_{22}$ translate into different melt specific volumes. The LCT, in contrast, treats structured monomers, which allows a compensating coupling between asymmetric energies and monomer structure. Thus, for example, the more branched monomer in a binary blend can be given a higher ϵ_{11} than the other component in order to make both melts have the same specific volumes. The influence of compressibility then appears in the form of contributions involving the energy differences $\epsilon_{12} - \epsilon_{11}$, etc.

The present work represents a continuation of our previous paper[20] to assess the relative importance of factors suggested by prior theories and models as affecting polyolefin miscibilities. These factors include stiffness and interaction disparities, local monomer structures, nonrandom mixing, and compressibility, all of which are studied by utilizing the extension of the LCT to describe the statistical thermodynamics of semiflexible lattice polymers.[21] Bawendi and Freed[22] provide only a leading order treatment of chain semiflexibility within the original field theory formulation of the LCT. Subsequent work,[23] however, demonstrates that the next order contributions are necessary for flexible chain models in order for the LCT to agree with simulations. Thus, we employ the previous model in which chain semiflexibility is described by introducing an energy difference between trans and gauche conformations for a pair of consecutive bonds in a chain. The extension of the LCT to provide the important next order contribututions is rather nontrivial and technically involved, so the details will be presented elsewhere.[21]

Reference 20 focuses solely on blends of semiflexible linear lattice chains in order to provide direct comparisons with PRISM computations. The near identity of LCT and PRISM computations for the influence of stiffness disparity on blend miscibilities provides further credence that the extended lattice model captures all the essential physics generally expected only in off-lattice models and that the LCT is therefore worth developing for application to experimental data. The computations in ref 20 concur with previous suggestions that both semiflexibility and the exchange energy ϵ_{ex} significantly influence miscibility patterns. Therefore, the present work provides the extension of ref 20 to consider semiflexibility for chains of structured monomers within a united atom model. One interest lies in determining whether the linear $(T_c/M) - r^2$ correlation of Dudowicz and Freed persists when the structured monomer chains are endowed with variable semiflexibility. Hence, the present computations represent the first treatment of polyolefin miscibilities which combines nonrandom mixing, monomer structures, noncombinatorial corrections to the entropy, asymmetric van der Waals energies, and semiflexibility within the same model.

Section II begins by very briefly describing the semiflexible chain lattice model and the LCT. Section II concludes with highly nontrivial calculations for the radius of gyration R_G for the semiflexible lattice polymers with the arbitrary topologies that apply to models with structured monomers. The radius of gyration for the structured semiflexible lattice chains is essential for computing the stiffness disparity parameter and, hence, for directly comparing with either PRISM computations or the predictions of the BF model. Appendix A explains the derivation of the general formulae for the R_G of these structured monomer lattice chains. Section III begins with a test of various claims concerning the miscibilities of polyolefin blends. The oversimplified BF model is shown to be an inadequate predictor of polyolefin blend miscibilities. The LCT computations further suggest that the modeling of real (branched) chains by thermodynamically equivalent linear semiflexible chains requires a delicate balancing of several factors. Since the chain topology (i.e., monomer structures) distinctly influences the blend miscibility, the remarkable linear $(T_c/M) - r^2$ correlation of Dudowicz and Freed is extended to include chain semiflexibility, with quite excellent results. This extended correlation supports the utility of the LCT to describe experimental phenomena. Section IV analyzes the influence of asymmetric van der Waals interactions on the miscibilities of semiflexible blends and the important pressure dependence of their phase diagrams. Comparisons are provided between LCT and experimental phase diagrams for some polyolefin blends studied by Graessley, Lohse, and co-workers. Particular emphasis is placed on PIB-containing blends whose phase behavior deviates from solubility parameter models and which exhibit an anomalous dependence on molecular weight that is explained here. Elsewhwere we will present computations for the nearest neighbor contact probabilities[21b] that reflect the significant nonrandom mixing contributions contained in the LCT.

II. Lattice Cluster Theory of Semiflexible Binary Blends

A. Lattice Model. We employ a d-dimensional cubic lattice model with N_l lattice sites, each with $z = 2d$ nearest neighbors. This d-dimensional lattice is used within our theory to develop expansions of the free energy in $1/z$, but all computations are performed for $d = 3$ dimensions. The example of polyolefin systems provides a simple motivation for the extended lattice model which prescribes specified monomer structures. The CH_n $(n = 0-3)$ groups of each polyolefin chain are represented as united atom groups, each of which occupies one lattice site and has the volume v_c (=17 Å^3). Excluded volume constraints prohibit simultaneous occupation of a lattice site by more than one united atom group. Hence, the individual monomers of species α occupy $s_\alpha > 1$ lattice sites. The monomer structures considered in this paper are depicted in Figure 1. United atom groups that are bonded to only one other united atom group in the chain are called terminal groups. For example, the two chain ends and all side chain united atom groups in Figure 1 are termini. All the branched topologies in Figure 1 contain at least one terminus per monomer. Species i has $n_p(i)$ chains with M_i united atom groups per chain, producing the volume fraction $\phi_i = n_p(i)M_i/N_l$.

Semiflexibility for linear chains is treated[21] by introducing an energy penalty $E_b(i)$ for pairs of consecutive bonds in a single chain from species i whenever the pair

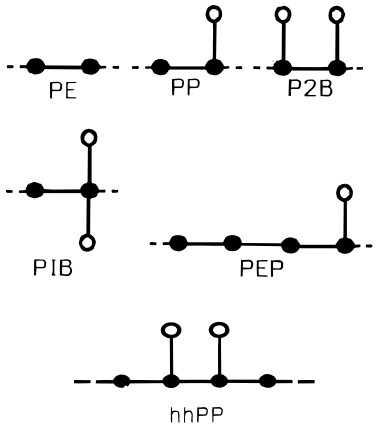

Figure 1. United atom representations for portions of polyethylene (PE), polypropylene (PP), poly(2-butene) (P2B), polyisobutylene (PIB), poly(ethylenepropylene) (PEP), and head-to-head polypropylene (hhPP). Circles denote CH_n $(n = 0-3)$ groups occupying single lattice sites. Filled and open circles indicate backbone and side chain groups, respectively. Each side chain group is a terminus because it is bonded to only one other united atom group in the chain.

of bonds lies along orthogonal lattice directions (called the "gauche" conformation) as displayed in Figure 2. No bending energy is assigned when the pair of consecutive bonds consists of one backbone bond and one side chain bond. Thus, a propyl monomer in a chain contains one trifunctional united atom group and is assigned one bending energy for "gauche" conformations of the two consecutive backbone bonds. The isobutyl monomer in a chain contains a tetrafunctional united atom group and is, therefore, assigned two different bending energies, one for "gauche" conformations of the pair of backbone bonds and one for the "gauche" conformations of the consecutive pair of side chain bonds eminating from the single tetrafunctional united atom group as depicted in Figure 2. Although the backbone and side-chain bending energies may differ, all bending energies for a given species are taken as equal, for simplicity. The longer range interactions are modeled by introducing attractive nearest neighbor van der Waals energies $\epsilon_{ij}^{\alpha\beta}$, where i and j represent the chain species of the two interacting united atom groups and α and β designate the specific pair of united atom groups within the monomers. In order to minimize the number of parameters, all united atom groups from species i and j are assumed to interact with the same energy ϵ_{ij}, leaving only three independent interaction energies for a binary blend. Once again, our theoretical approach can include group specific interaction energies[21a] if warranted by experimental data, but this inclusion occurs at the expense of additional parameters or assumptions.

While many models of blend thermodynamics assume incompressibility, compressibility is, in fact, required to investigate the technologically important pressure dependence. Compressible blends contain excess free volume, which is described by including a fraction ϕ_v of unoccupied sites. The fraction ϕ_v is determined from the equation of state for a given pressure, temperature, blend composition, and unit cell volume. The binary blend composition is expressed in terms of the nominal volume fractions $\Phi_i = \phi_i/(1 - \phi_v)$, with $\Phi_1 + \Phi_2 = 1$. We set $\Phi \equiv \Phi_1$ for notational simplicity in presenting the figures.

B. Thermodynamic Quantities. The lattice cluster theory (LCT) yields the Helmholtz free energy F of

Table 1. Counting Factors $N_{n+1,s}$ for Structrures in Figure 1[a]

	PP	P2B	PIB	PEP	hhPP
$N_{2,1}$(b,b)	$9\rho(\rho^2-1)/6$	0	$16\rho(\rho^2-1)/6$	$\rho(75\rho^2-15)/6$	$\rho(72\rho^2-42)/6$
$N_{2,2}$(b,b)	$\rho(9\rho^2-9\rho+6)/6$	$\rho(32\rho^2+4)/6$	0	$(25\rho^3-15\rho^2+8\rho)/6$	$(72\rho^3-36\rho^2+24\rho)/6$
$N_{2,2}$(b,s)	$\rho(3\rho-1)$	$8\rho^2$	0	$\rho(5\rho-1)$	$\rho(12\rho-2)$
$N_{2,3}$(b,b)	0	0	$(16\rho^2-24\rho+14)/6$	0	0
$N_{2,3}$(b,s)	0	0	$4\rho(2\rho-1)$	0	0
$N_{2,3}$(s,s)	0	0	ρ	0	0
$N_{3,1}$(b,b)	$9\rho(\rho-1)^2/6$	0	0	$\rho(50\rho^2-30\rho-2)/6$	$\rho(\rho-1)(36\rho+18)/6$
$N_{3,2}$(b,b)	$9\rho(\rho-1)^2/6$	0	0	$\rho(50\rho^2-60\rho+22)/6$	$\rho(72\rho^2-90\rho+30)/6$
$N_{3,2}$(b,s)	$3\rho(\rho-1)$	0	0	$\rho(5\rho-3)$	$6\rho^2-5\rho$
$N_{3,3}$(b,b)	0	$(32\rho^3-48\rho^2+28\rho-6)/6$	0	0	$\rho(36\rho^2-54\rho+30)/6$
$N_{3,3}$(b,s)	0	$8\rho^2-4\rho-2$	0	0	$6\rho^2-3\rho$
$N_{3,3}$(s,s)	0	$2\rho-1$	0	0	ρ
$N_{3,4}$(b,b)	0	0	$8\rho(\rho-1)(4\rho-5)/6$	0	0
$N_{3,4}$(b,s)	0	0	$8\rho(\rho-1)$	0	0
$N_{4,1}$(b,b)	0	0	0	$5\rho(5\rho-1)(\rho-1)/6$	0
$N_{4,2}$(b,b)	0	0	0	$(50\rho^3-90\rho^2+58\rho-12)/6$	$(\rho-1)(72\rho^2-36\rho+12)/6$
$N_{4,2}$(b,s)	0	0	0	$5\rho^2-5\rho+1$	$(6\rho-1)(\rho-1)$
$N_{4,3}$(b,b)	$9\rho(\rho-1)(\rho-2)/6$	0	0	$5\rho(5\rho-4)(\rho-1)/6$	0
$N_{4,4}$(b,b)	$(\rho-1)(9\rho^2-27\rho+24)/6$	0	0	0	0
$N_{4,4}$(b,s)	$(3\rho-4)(\rho-1)$	0	0	0	0
$N_{4,4}$(s,s)	$\rho-1$	0	0	0	0
$N_{4,5}$(b,b)	0	0	0	0	$\rho(72\rho^2-144\rho+78)/6$
$N_{4,5}$(b,s)	0	0	0	0	$6\rho^2-5\rho$
$N_{4,6}$(b,b)	0	$(\rho-1)(32\rho^2-64\rho+36)/6$	0	0	0
$N_{4,6}$(b,s)	0	$8(\rho-1)^2$	0	0	0
$N_{4,6}$(s,s)	0	$2(\rho-1)$	0	0	0
$N_{4,7}$(b,b)	0	0	$16\rho(\rho-1)(\rho-2)/6$	0	0
$N_{4,8}$(b,b)	0	0	$(\rho-1)(16\rho^2-56\rho+54)/6$	0	0
$N_{4,8}$(b,s)	0	0	$4(2\rho-3)(\rho-1)$	0	0
$N_{4,8}$(s,s)	0	0	$4(\rho-1)$	0	0

[a] ρ represents the polymerization index for the polymer listed at the top of the column and is equal to $(M-1)/3$, $(M-2)/4$, $(M-1)/4$, $(M-1)/5$, and $(M-1)/6$ for PP, P2B, PIB, PEP, and hhPP, respectively.

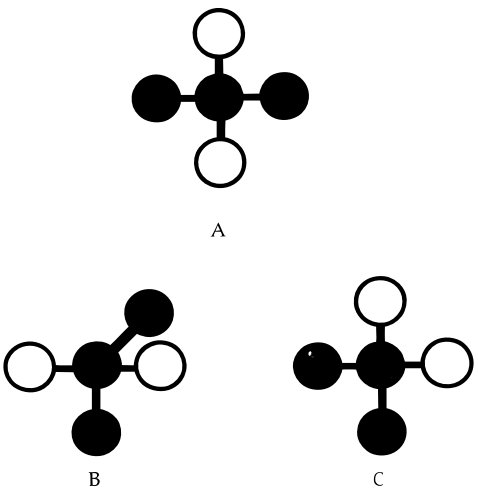

Figure 2. Trans−trans (A), trans−gauche (B), and gauche−gauche (C) conformations of the isobutylene monomer. Filled and open circles designate backbone and side chain groups, respectively. In each configuration, bends between any pair of connected bonds are assigned an energy penalty E_b, except when the pair consists of one backbone bond and one side chain bond (those that lie along the topologically forced bends). This four bond structure has N_{2s} (=2) and N_{2b} (=4) consecutive bonds which are assigned a bending energy penalty of E_b and of 0, respectively, for the gauche conformation. Hence, configurations A, B, and C have energy penalties of 0, E_b, and $2E_b$, respectively. Identical rules are employed to assign energy penalties to the other structures in Figure 1.

a binary blend in the general form

$$\frac{F}{N_1 k_B T} = \phi_v \ln \phi_v + \sum_{i=1}^{2} \frac{\phi_i}{M_i} \left\{ \ln\left(\frac{2\phi_i}{zM_i}\right) - N_{2,s}(i) \ln[z_b(i)] + N_1(i) \right\} + \sum_{i=0}^{6} \sum_{j=0}^{6-i} c_{ij} \phi_1^{\,i} \phi_2^{\,j} \quad (2.1)$$

where

$$z_b(i) = (z-1) \exp\left(\frac{-E_b(i)}{k_B T}\right) + 1$$

k_B is Boltzmann's constant, T is the absolute temperature, $N_1(i)$ is the number of bonds in a single chain of species i, while $N_{2,s}(i)$ the number of pairs of consecutive bonds that are assessed an energy penalty when any of them are in gauche configurations (see eq 3.5 for a precise definition). The $\{c_{ij}\}$ are coefficients that are presented in ref 20 for linear chains, and the general case will be given elsewhere[21a] for multicomponent blends of arbitrary structured semiflexible chains, along with the lengthy derivation of eq 2.1. The first two terms on the right hand side of eq 2.1 provide the combinatorial portion of F. When all the $E_b(i)$ vanish and only the leading random mixing terms are retained, eq 2.1 reduces to a compressible generalization of the Flory−Huggins type free energy expression, with an explicit portion of the noncombinatorial entropy. The last term in eq 2.1 provides both the leading random mixing type term and the important nonrandom mixing corrections. The double sum in eq 2.1 is computed as a polynomial in the volume fractions ϕ_1 and ϕ_2. The coefficients c_{ij} in eq 2.1 are generated through second order in a double expansion in $1/z$ and $\epsilon_{ij}/k_B T$ as in previous developments of the purely flexible chain LCT [24] which employ truncations of the order $(\epsilon_{ij}/k_B T)^2$. The coefficients in this expansion are now functions of the bending energy through the factor

$$g_i \equiv \frac{z \exp\left(\frac{-E_b(i)}{k_B T}\right)}{z_b(i)} \quad (2.2)$$

which is assigned a formal order of unity as in the work of Bawendi and Freed.[22]

Many experiments are performed at constant pressure. The pressure P is obtained from the free energy

F as

$$P = -\left.\frac{\partial F}{\partial V}\right|_{T,n_1,n_2} \tag{2.3}$$

where $V \equiv N_1 v_c$. Constant pressure spinodals are then determined from the usual thermodynamic stability condition,[19]

$$\left.\frac{\partial \mu_1}{\partial \Phi}\right|_{T,P} = 0 \tag{2.4}$$

where the chemical potential μ_1 (per unit segment) is given by

$$\mu_1 = \left.\frac{1}{M_1}\frac{\partial F}{\partial n_1}\right|_{T,V,n_{j\neq 1}} \tag{2.5}$$

The calculation of binodals is also possible, but the computationally simpler spinodals display all miscibility trends. Experimental data for the isothermal compressibility κ are used to determine the homopolymer van der Waals energy and κ is derived from the expression for the pressure eq 2.3 as

$$\kappa^{-1} = -V\left.\frac{\partial P}{\partial V}\right|_{T,n_1,n_2} \tag{2.6}$$

C. Stiffness Disparity Parameters. Differences in chain stiffness can greatly influence the phase behavior of binary polymer blends, and ref 20 demonstrates, not surprisingly, that an equally important influence is provided by the exchange energy ϵ_{ex} in eq 1.1. The present work studies how the monomer structures cooperatively act with ϵ_{ex} and with stiffness disparities to influence blend phase behavior. Section III uses the LCT to provide a partial test of the thermodynamically equivalent chain model of Schweizer and co-workers.[13,15−17] Since we cannot yet obtain the full pair distribution function for the extended lattice model, the spirit of Schwieizer's model is partially satisfied by choosing the bending energy of a linear chain to make the respective aspect ratios for the structured monomer chain and semiflexible linear chain as equal as possible.

Comparisons with the work of Schweizer and coworkers require considering the aspect ratio which is defined for the off-lattice models as the ratio of the Kuhn length a to the hard sphere diameter d. Since the lattice constant $L = v_c^{1/3}$ is identical for all lattice chains and is the natural lattice model analog of d, the LCT analog of the stiffness disparity parameter ξ simplifies to the difference in Kuhn lengths a_i of the two blend components divided by their average

$$\zeta_{LCT} = 2\frac{a_2 - a_1}{a_2 + a_1} \tag{2.7}$$

Hence, the determination of the stiffness disparity ξ reduces to evaluation of the individual a_i. The Kuhn lengths for each species are calculated from the mean squared radii of gyration $\langle R_G^2\rangle$ for the components. In the long chain, Gaussian limit, the Kuhn length a is related to $\langle R_G^2\rangle$ by

$$\langle R_G{}^2\rangle = a^2\frac{n_a}{6} \tag{2.8}$$

where n_a, the number of Kuhn segments, is taken here, for simplicity, as the polymerization index. Comparisons with the BF model, on the other hand, are facilitated by considering their stiffness parameter $\beta = \langle R_G^2\rangle/V_m$, where V_m is the total occupied volume of the chain. Since V_m in the lattice model is proportional to M, an alternative stiffness parameter may be defined with M replacing n_a in eq 2.8, but the same general conclusions emerge from using either definition. Reference 20 presents computations of ξ_{LCT} for semiflexible linear lattice chains, but the extension here to structured monomers is technically quite involved. Readers more interested in the results might skip directly to section III.

D. Radius of Gyration for a Single Chain. Since polymers at liquidlike densities have only short-range memory of intramolecular correlations, $\langle R_G^2\rangle$ is determined for a single nonreversing random walk, a model which reasonably approximates the results from Monte Carlo simulations of linear polymers in melts.[25,26] The derivation of an expression for $\langle R_G^2\rangle$ begins with the general expression of Zimm and Stockmayer,[27] which has been derived for arbitrary branched structures as

$$\langle R_G{}^2\rangle = \frac{1}{M^2}\sum_{i<j=1}^{M}\langle \mathbf{r}_{ij}{}^2\rangle \tag{2.9}$$

where $\mathbf{r}_{ij}$ is the vector between united atom groups i and j in the chain. The numbering of the united atom groups for a given chain architecture is somewhat arbitrary, requiring only that each group be assigned a unique integer between 1 and M. The precise numbering scheme is, therefore, not detailed here. Chains with no closed loops have the topological property that a unique path exists between any two points on the chain such that the path traverses bonds only once. Hence, the displacement vector $\mathbf{r}_{ij}$ is composed of the sum of the bond vectors $\{\mathbf{b}_k\}$ that lie along the unique connecting path between monomers i and j. Thus, we may write

$$\mathbf{r}_{ij} = \sum_{k=1}^{N_b(i,j)}\mathbf{b}_k \tag{2.10}$$

where $N_b(i,j)$ is the number of bonds between united atom groups i and j along the connecting path. For example, linear chains with sequentially labeled monomers yield $N_b(i,j) = |i - j|$. Substituting eq 2.10 into eq 2.9 produces

$$\langle R_G{}^2\rangle = \frac{1}{M^2}\sum_{i<j=1}^{M}\sum_{k=1}^{N_b(i,j)}\langle \mathbf{b}_k\cdot\mathbf{b}_{k'}\rangle \tag{2.11}$$

where the sums on k and k' run over the appropriate bonds along the connecting path between united atom groups i and j. Equation 2.11 is exact for a single chain of arbitrary architecture and polymerization index, regardless of the model used.

Each bond vector $\mathbf{b}_k$ in the lattice model is the product of the step length $L = (v_c)^{1/3}$ and a unit vector along one of the three orthogonal lattice directions, where v_c is the cell volume. This fact permits a factor of L^2 to be removed from the sum in eq 2.11, with the remaining averaged scalar product containing unit vectors. Only scalar products between parallel or antiparallel unit bond vectors produce nonzero contributions to the averages in the summations of eq 2.11. Further, whenever the summation indices k and k' in eq 2.11 are equal, the contribution is always unity since any bond vector is parallel to itself. Hence, eq 2.11 may be rewritten as

$$\langle R_G^2\rangle = \frac{L^2}{M^2}\sum_{i<j=1}^{M}[N_b(i,j) + 2\sum_{k<k'=1}^{N_b(i,j)}\langle\delta(\mathbf{b}_k - \mathbf{b}_{k'}) - \delta(\mathbf{b}_k + \mathbf{b}_{k'})\rangle] \quad (2.12)$$

where δ is the Kronecker delta which equals unity when its argument vanishes. The two Kronecker deltas in the average in eq 2.12 arise from parallel and antiparallel orientations of the two bond vectors $\mathbf{b}_k$ and $\mathbf{b}_{k'}$.

The exact calculation of the mean squared radius of gyration in eq 2.12 is extremely difficult for all but the random walk model. Since only short range memory remains for a non-reversing random walk, we retain in the expansion of eq 2.12 for $\langle R_G^2\rangle$ only those contributions from correlations between bonds $\mathbf{b}_k$ and $\mathbf{b}_{k'}$ that are close to each other. "Close bonds" are defined for the present purpose as those which have two or less intervening bonds between them (i.e., for $|k - k'| \leq 3$ in eq 2.12) on the connecting path. This restriction reduces eq 2.12 to the more manageable form

$$\langle R_G^2\rangle = \frac{L^2}{M^2}\sum_{i<j=1}^{M}\{N_b(i,j) + 2[\vartheta(N_b(i,j) - 1)\times \sum_{k=1}^{N_b(i,j)-1}\langle\delta(\mathbf{b}_k - \mathbf{b}_{k+1}) - \delta(\mathbf{b}_k + \mathbf{b}_{k+1})\rangle + \vartheta(N_b(i,j) - 2)\times \sum_{k=1}^{N_b(i,j)-2}\langle\delta(\mathbf{b}_k - \mathbf{b}_{k+2}) - \delta(\mathbf{b}_k + \mathbf{b}_{k+2})\rangle + \vartheta(N_b(i,j) - 3)\times \sum_{k=1}^{N_b(i,j)-3}\langle\delta(\mathbf{b}_k - \mathbf{b}_{k+3}) - \delta(\mathbf{b}_k + \mathbf{b}_{k+3})\rangle]\} \quad (2.13)$$

where the Heaviside function $\vartheta(x)$ is unity if $x > 0$ and is zero otherwise.

Each average $K_n = \langle\delta(\mathbf{b}_k - \mathbf{b}_{k+n}) - \delta(\mathbf{b}_k + \mathbf{b}_{k+n})\rangle$ represents the exact correlation between the "starting" $\mathbf{b}_k$ and the "ending" $\mathbf{b}_{k+n}$ bonds which lie at the termini of an $n + 1$ step connecting path between these bonds. In order to evaluate the averages K_n, it is only necessary to consider the configurations for a small portion of the whole chain. This chain portion contains all bonds in the connecting path from $\mathbf{b}_k$ to $\mathbf{b}_{k+n}$, as well as some additional bonds attached to the united atom groups intermediate along this connecting path. The extra bonds are determined in a two-step process as follows: for given n, begin at the starting bond $\mathbf{b}_k$ and construct all paths, called extra paths, of length $n + 1$ bonds. If, in constructing these extra paths, a chain end or side chain terminus is encountered, include these extra paths even when the extra paths contain less than $n + 1$ bonds. A separate set of extra paths is also constructed starting from the ending bond $\mathbf{b}_{k+n}$. Define the set of "essential" bonds as containing those bonds appearing at least once in both sets of extra paths. The union of the bonds along the connecting path with the essential bonds compose a "local structure" for a path of length $n + 1$ bonds. The average K_n is computed by performing the indicated average over all possible configurations of the appropriate local structure. Figure 3 depicts the relevant local structures for computing K_1, K_2, and K_3 for the monomer structures in Figure 1. Monomers with topologies different from those in Figure 1 may require additional local structures not depicted in Figure 3.

Now consider the properties of a given local structure. The average correlation between the starting bond $\mathbf{b}_k$ and the ending bond $\mathbf{b}_{k+n}$ in a given local structure is independent of where or of how often the particular local structure is found in a chain; i.e., the average correlation K_n between bonds at the ends of the connecting path is not influenced by bonds that are not included in the local structure. Hence, the average correlation between $\mathbf{b}_k$ and $\mathbf{b}_{k+n}$ is exclusively a function of the given local structure. We denote the average correlation K_n between starting and ending bonds in a local structure as $W_{n,s}$, where n is the connecting path length and s denotes the specific local structure (cf., Figure 3). A local structure, such as structure a2 of Figure 3, yields two separate contributions, $W_{2,1}$(b,b) and $W_{2,2}$(b,s), which correspond, respectively, to cases where $\mathbf{b}_k$ and $\mathbf{b}_{k+1}$ are both backbone bonds and where one of the two bonds lies along the side-chain. Let $W_{n,s}(\alpha,\beta)$ separately designate the different possible averages from the same local structure for different pairs of starting and ending bonds. The variables α and β label the starting and ending bonds, respectively, with "b" and "s" designating backbone and side-chain bonds, respectively. A more complicated labeling scheme is necessary for polymers with more extended side chain structures and is not described here.

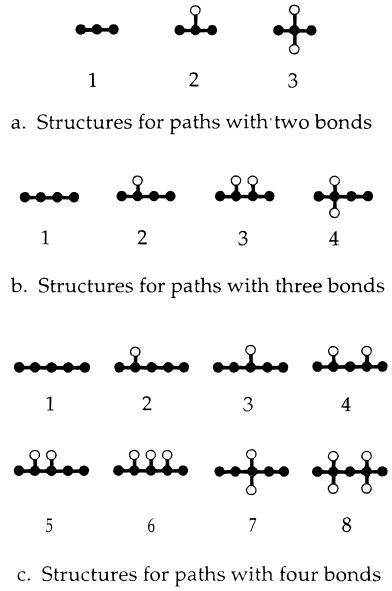

Figure 3. All unique topological structures used to determine average correlations $\{W\}$ in eq 2.14 for the mean squared radius of gyration $\langle R_G^2\rangle$. Open and filled circles represent united atom groups on side chains and on the backbone, respectively.

That the average correlation between $\mathbf{b}_k$ and $\mathbf{b}_{k+n}$ depends only on the local structure proves useful in computing the averages in eq 2.13. Several different local structures contribute to the sums over k for a given pair of monomers i and j. When n is fixed, however, the average K_n is defined as the quantity $W_{n+1,s}(\alpha,\beta)$, for the appropriate s, α, and β. The existence of an equality between K_n and some $W_{n+1,s}(\alpha,\beta)$ still holds as i and j are varied. Hence, the sums over i, j, and k in eq 2.13 are replaced with sums over the connecting path length n, all possible contributions from each local structure ($s = 1, 2, ..., T_n$), where T_n is the total number of local structures for a given n, and all possible combinations (α,β) of starting and ending bonds for the local structure. The final result, presented explicitly below, involves a summation over all the $W_{n+1,s}(\alpha,\beta)$ that contribute to eq 2.13 (cf., Figure 3). The latter summation is multiplied by a counting factor $N_{(n+1),s}(\alpha,\beta)$ that equals the number of all pairs of united atom groups i and j in the whole polymer chain such that the connecting path between i and j both traverses the local

structures and includes the pair of bonds $\mathbf{b}_k$ (the α bond) and $\mathbf{b}_{k+n}$ (the β bond), for all possible placements of the local structure within the chain. The shortest connecting path between i and j is the one originating on $\mathbf{b}_k$ and terminating on $\mathbf{b}_{k+n}$.

The first sum in eq 2.13 [containing $N_b(i,j)$ as the summand] can be recast in terms of a $W_{1,1}(\alpha,\alpha)$ (=1), but this is unnessary because the sum is merely the $\langle R_G^2\rangle_{FJ}$ for an equivalent freely jointed (branched) chain. Yamakawa[28] presents the exact expression for this $\langle R_G^2\rangle_{FJ}$ of freely jointed chains with arbitrary architecture. Hence, we evaluate this first sum separately before changing the summations in eq 2.13. For notational simplicity, we define Δ by $\langle R_G^2\rangle_{FJ} = L^2\Delta/M^2$. Appendix A summarizes the exact expression for Δ for each of the polymers whose monomers are depicted in Figure 1. The final form for the approximate $\langle R_G^2\rangle$ is

$$\langle R_G^2\rangle = \frac{L^2}{M^2}\{\Delta + 2[\sum_{n=1}^{3}\sum_{s=1}^{T_n}\sum_{(\alpha,\beta)} N_{n+1,s}(\alpha,\beta)W_{n+1,s}(\alpha,\beta)]\} \tag{2.14}$$

where the contribution from each n provides the total contribution from all connecting paths of length $n + 1$ bonds, while the sum over s includes the contributions from all T_n unique local structures (see Figure 3) for fixed n. (The approximation in eq 2.14 arises from the truncation of the sum over n to an upper limit of $n = 3$.) Appendix A provides all formulae for the averages $\{W\}$ and for the counting factors $\{N\}$ used in the present study, as well as an example of how the $\{N\}$ and $\{W\}$ are evaluated.

III. Comparisons with Previous Models and Theories

Several mutually conflicting models have been developed to predict the phase behavior of binary polyolefin homopolymer blends. Subsection A below describes tests of the BF model, subsection B addresses approximations involved in the thermodynamically equivalent semiflexible linear component chain model, and subsection C extends to polyolefin blends of semiflexibile chains the remarkable relationship of Dudowicz and Freed between the critical temperature T_c, the total number of united atom groups M, and the fraction of tri- and tetrafunctional carbons in the chains. The present LCT computations suggest that most proposed models for predicting polyolefin miscibility suffer from at least minor deficiencies, with the semiflexible LCT being no exception. The deficiencies of the generalized, semiflexible chain lattice model are shown to be overcome easily, permitting the prediction of the miscibility of some binary homopolymer polyolefin blends. Section IV relates the LCT computations to experimental data.

A. The Bates−Fredrickson Model. We explicitly test the assertion of the BF model[8−12] that stiffness disparity alone is the primary determinant of miscibility by considering binary blends consisting of a semiflexible linear chain (a model of PE) as component 1 and one of the branched polymers in Figure 1 as component 2. All united atom groups are assigned the identical van der Waals energies ($\epsilon_{ij} = \epsilon$), producing a vanishing exchange energy ϵ_{ex}. (Nonzero ϵ_{ex} are considered in section IV.) Our use of a common interaction energy for all species coincides with the total neglect of enthalpic differences in the BF model and with the need for including attractive interactions to produce typical liquid densities at ambient pressures. As in prior PRISM and in semiflexible LCT[20] computations, the global miscibility pattern is summarized using isothermal phase diagrams that present the rescaled minimum number $(1 - \phi_v)M_c$ of united atoms needed for producing phase separation in a binary blend (with $M_1 = M_2 = M_c$) as a function of the stiffness disparity parameter ξ of eq 2.7. As in ref 20, this M_c is scaled by $(1 - \phi_v)$ to eliminate the variation of the phase diagrams with density and to produce a universal curve for all excess free volume fractions ϕ_v that yield liquidlike densities. The bending energy for the PE component is varied from $-10k_BT$ to $+10k_BT$, a range which generates PE topologies from completely kinked chains to rigid linear rods, respectively, with flexible chains in between [at $E_b(PE) = 0$]. If stiffness disparity is the primary parameter governing blend miscibility, the phase diagrams should indicate complete miscibility as ξ approaches 0.

Figure 4a exhibits phase diagrams for the semiflexible PE blended separately with each of the five other flexible branched polymers of Figure 1. A vanishing ξ (when achieved) does not yield complete miscibility (which implies $M_c \rightarrow \infty$) for any of these cases, confirming that semiflexibility is but one of several factors that determine miscibility and, at best, provides only a qualitative guide to determining phase behavior. All the model binary blends considered in Figure 4 yield maximal miscibility (i.e., largest M_c) when the PE chains are given extremely negative bending energies and, hence, when ξ is far from zero. Large negative bending energies favor bent or kinked conformations in the PE component. A highly bent chain experiences a larger intrachain excluded volume effect, much like a chain with a branched architecture. Hence, miscibility is expected to increase with increasingly negative bending energies, as is evident in Figure 4b. The model blends in Figure 4 never achieve complete miscibility, even when using a large negative bending energy for the linear chain component, thereby suggesting that the stiffness of the linear semiflexible chain cannot be adjusted such that it produces identical excluded volume constraints as a structured monomer chain (when all unit cell volumes remain fixed). This finding accords with the use by Schweizer and co-workers of several constraints in adjusting both the stiffness disparity and the pair distribution functions.

In the spirit of the BF model, we now consider the phase behavior of binary blends whose components have equal polymerization indices (instead of equal numbers of united atom groups). Figure 5 considers the same model blends as in Figure 4 and illustrates that the restriction to equal polymerization indices leads to qualitatively different phase behaviors than in Figure 4a. Nevertheless, the blends do not automatically become more miscible as the stiffness disparity vanishes. The P2B/PE blend appears to reach maximal miscibility for $\xi = 0$, but all the other blends in Figure 5 exhibit the highest miscibility at either positive or negative ξ. The computations of Figures 4 and 5 may also be presented as a function of the disparities in the BF stiffness parameter asymmetry, i.e., in terms of $\langle R_G^2\rangle/M$, but the general conclusions are unchanged. The highest miscibilities then appear in the analog of Figure 5 for positive stiffness disparity parameters. The differences in molecular weights and monomer structures combine with the stiffness disparity to influence the phase behavior of polyolefin blends in a fashion that cannot be captured sufficiently by the BF model, which predicts complete miscibility for vanishing stiffness disparity $\xi = 0$.

Although Monte Carlo simulations[25,26] suggest that the mean squared radius of gyration $\langle R_G^2\rangle$ for linear

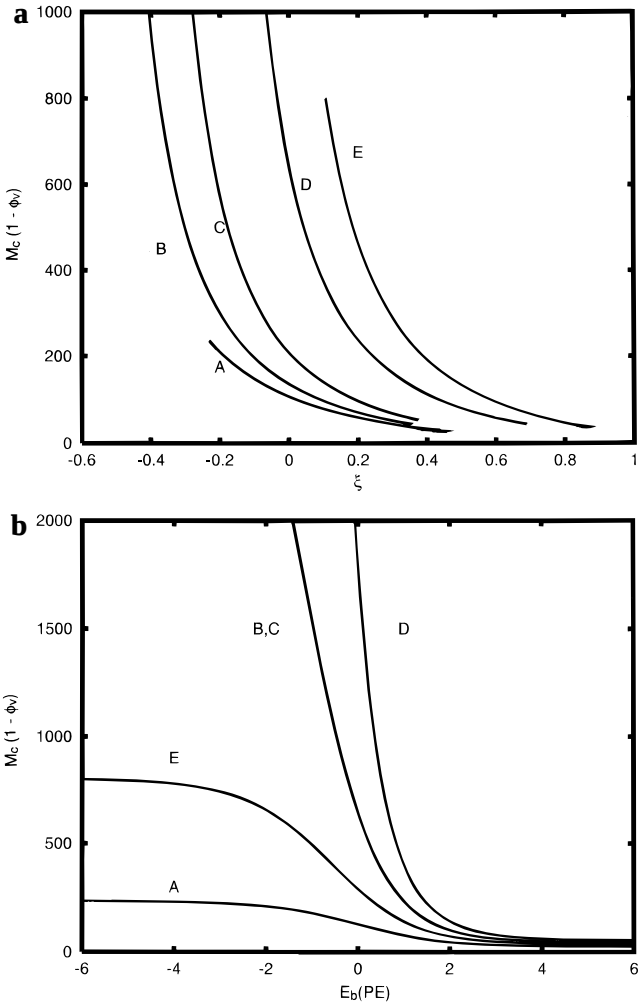

Figure 4. Global phase diagrams depicting the rescaled minimum number $(1-\phi_v)M_c$ of united atom groups necessary for phase separation as a function either of (a) the stiffness disparity ξ or (b) of the dimensionless bending energy E_b(PE)/k_BT for PE. The global phase curves are for systems of PE blended with PIB (A), hhPP (B), PEP (C), PP (D), and P2B (E). All calculations are for $\Phi = 0.5$, all equal van der Waals energies $\epsilon_{ij}/k_B = 0$ K, and temperature fixed at $T = 300$ K. The second component is always PE. The bending energy of the branched component is set at 0 K, while the bending energy for PE is varied. Rescaling M_c by $(1-\phi_v)$ produces a single universal curve for all $\phi_v \leq 0.25$ (i.e., for liquidlike densities). Part a illustrates that vanishing stiffness disparity ($\xi = 0$) does not yield a completely miscible blend ($M_c \rightarrow \infty$). Rather, miscibility increases in part b as the bending energies become more negative, although complete miscibility is never reached (curves B and C level off between 3900 and 4000, while curve D levels off at 4×10^5). The inability to achieve complete miscibility strongly suggests that semiflexible linear chains cannot completely model the behavior of structured monomer (branched) chains.

polymers in the bulk is well approximated by an $\langle R_G^2 \rangle$ for the equivalent nonreversing random walk (NRRW), real polymers cannot self-intersect, a feature better modeled by self-avoiding walks (SAWs). Therefore, we have also determined the $\langle R_G^2 \rangle$ and, hence, the stiffness disparity parameters ξ_{SAW} from an equivalent self-avoiding walk (SAW) with short range memory in which four-bond square configurations are prohibited. (See Appendix A for more details.) All phase diagrams for the NRRW and the short-range SAW are nearly identical, except for the unphysical range of rather large, negative bending energies, where small deviations occur. The deviations arise because the only difference between the present computed $\langle R_G^2 \rangle$ for a NRRW and for a short range SAW emerge from four-bond closed

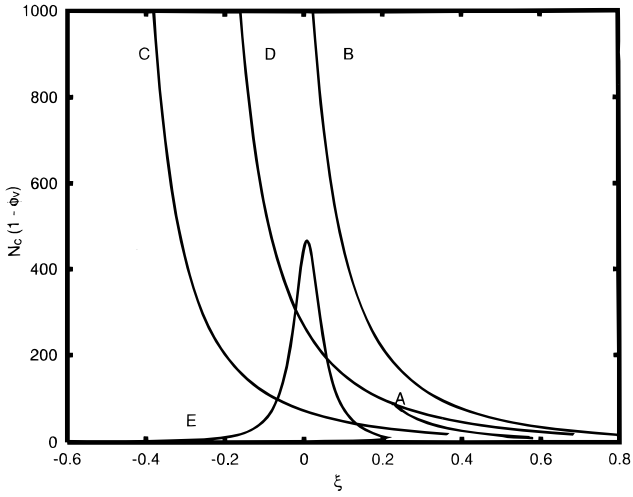

Figure 5. Same as Figure 4a, except now displaying the rescaled minimum polymerization index $N_c(1-\phi_v)$ as a function of ξ. Immiscibility does not disappear ($N_c \rightarrow \infty$) with vanishing ξ but instead requires complex interplay between polymer topology and bending energy differences.

loop structures (squares) which are permitted in the former and are forbidden in the latter. These squares provide relatively small corrections to the $\langle R_G^2 \rangle$ for flexible or rigid chains but become more significant for negative bending energies which increasingly favor chain kinking. The global phase diagrams using ξ_{NRRW} and ξ_{SAW} are nearly identical, suggesting that the more realistic inclusion of local excluded volume constraints does not restore complete miscibility for vanishing stiffness disparity.

B. Thermodynamically Equivalent Chain Model. The fact that a vanishing stiffness disparity does not produce complete miscibility directly bears on a model used by Schweizer and co-workers to describe polyolefin blend miscibilities. They apply PRISM integral equation methods to an off-lattice model of linear hard sphere chains whose stiffness is adjusted by use of a single bending energy parameter.[15] The stiffness of the linear chain in a melt is adjusted such that the intra- and intermolecular pair distribution functions for the semiflexible chain and for the corresponding real (branched semiflexible) chain are nearly identical at a single temperature. Once the intramolecular pair distributions functions, the aspect ratios, and the packing fractions are matched, the semiflexible linear chains are employed instead of the branched ones in the calculation of blend properties. This model directly implies that a blend of the semiflexible linear component with the corresponding branched component would be nearly completely miscible. We are unable here to determine if the intra- and intermolecular pair correlation functions are similar for the semiflexible linear chain and the flexible structured chain. Nevertheless, Figure 4 considers the full range of possible bending energies for PE (both positive and negative) and, therefore, must include the case where the intramolecular pair distributions are most nearly identical. Yet, no significant increase appears in the miscibility of the semiflexible linear/flexible branched blends for any values of E_b(PE).

C. Correlations with the Entropic Structural Parameter. The monomer structures and, more generally, the chain architechture greatly affect the miscibility of the LCT polyolefin binary blends. Dudowicz and Freed[18,19] show that the ratio T_c/M of the binary blend critical temperature T_c to the number $M = M_1 = M_2$ of united atom groups in individual chains varies

linearly with the square of the entropic structural parameter $r = |(N_2(1)/M_1) - N_2(2)/M_2|$

$$\frac{T_c}{M} = Ar^2 + B \tag{3.1}$$

where $N_2(i)$ is the total number of pairs of consecutive bonds in a chain of component i. Equation 3.1 applies to binary blends of chains with identical numbers of united atom groups ($M_1 = M_2 = M$) and with all van der Waals energies equal. The prior computations with all equal ϵ_{ij}, i.e., with $\epsilon_{ij}/k_B = 207.575$ K (where k_B is Boltzmann's constant), yield the coefficients A and B in eq 3.1 as $A = 5.06$ and $B = -0.031$. The blends studied by Dudowicz and Freed do not explicitly include bending energies [$E_b(i) = 0$], but no restriction is placed on the topologies of the two blend components. Since both PRISM computations and our LCT treatment emphasize the importance of semiflexibility in determining miscibility patterns (a point noted long ago by Flory[29]), it is clearly of interest to determine whether the strong correlation in eq 3.1 can be extended to incorporate the large influences of chain semiflexibility. Below, we generalize eq 3.1 to predict the trends in miscibility for blends of structured semiflexible polymers.

The correlation in eq 3.1 fails to describe LCT computations for blends when bending energies are introduced into the model. Thus, the structural parameter r [or equally, $N_2(i)$] must be recast in a form that includes the bending energy coefficients g_i of eq 2.2. The appropriate modification of r^2 for chains with bending energies may be deduced by considering the limiting high pressure ($P \to \infty$), high molecular weight ($M \to \infty$) noncombinatorial entropic contribution to the athermal binary blend free energy. This procedure suggests the new expression for $N_2(i)$

$$N_2(i) = N_{2s}(i)g_i + N_{2b}(i) \tag{3.2}$$

where N_{2s} and N_{2b} represent the total numbers of pairs of consecutive bonds which, respectively, are and are not assessed a bending energy penalty when the pair is in the gauche conformation. (Recall that no bending energy is assigned between a pair of backbone and side group bonds that share a common monomer.) The number $N_{2b}(i)$ is simply related to the numbers of tri- and tetrafunctional carbons ($M^{(i)}_{(tri)}$ and $M^{(i)}_{(tetra)}$, respectively) by

$$N_{2b}(i) = 2M^{(i)}_{(tri)} + 4M^{(i)}_{(tetra)} \tag{3.3}$$

The multiplicative factors on the right hand side of eq 3.3 arise from the fact that any trifunctional carbon contributes one "topologically forced bend" in which only one of the two consecutive bonds lies on a side chain. The side chain bond can be paired with either of the neighboring main chain bonds, yielding the factor of 2 in eq 3.3. A tetrafunctional carbon has two side chain bonds, each of which can pair with either of the two adjacent main chain bonds, thus producing the factor of 4 in eq 3.3. The number $N_{2s}(i)$ of pairs of consecutive bonds that are assessed an energy penalty when forming a gauche conformation can be derived by combining eq 3.2 for $g_i = 1$ with eq 3.3 and the previous general expression[18] of Dudowicz and Freed for $N_2(i)$ (of chains without bending energies)

$$N_2(i) = M_i - 2 + M^{(i)}_{(tri)} + 3M^{(i)}_{(tetra)} \tag{3.4}$$

producing the desired relation

$$N_{2s}(i) = N_2(i) - N_{2b}(i) = M_i - 2 - M^{(i)}_{(tri)} - M^{(i)}_{(tetra)} \tag{3.5}$$

Substituting eqs 3.3−3.5 into eq 3.2 allows the the entropic structural parameter r to be written as a function of the bending energy

$$r = \left|\frac{N_{2s}(1)g_1 + N_{2b}(1)}{M_1} - \frac{N_{2s}(2)g_2 + N_{2b}(2)}{M_2}\right| = \left|\frac{[M_1 - 2 - M^{(1)}_{(tri)} - M^{(1)}_{(tetra)}]g_1 + 2[M^{(1)}_{(tri)} + 2M^{(1)}_{(tetra)}]}{M_1} - \frac{[M_2 - 2 - M^{(2)}_{(tri)} - M^{(2)}_{(tetra)}]g_2 + 2[M^{(2)}_{(tri)} + 2M^{(2)}_{(tetra)}]}{M_2}\right| \tag{3.6}$$

Equations 3.3−3.6 are trivially evaluated by counting the number of different types of united atom groups in the monomer structures of Figure 1.

As in the work of Dudowicz and Freed, the combination of the expression in eq 3.6 for the structural parameter r with the correlation in eq 3.1 represents a significant generalization of an older rule of thumb that relates blend miscibilities to differences in the ratio p_i of end to total CH_n groups in a single chain of component i. Polyolefins with similar p_i have previously been believed to mix well, while large differences in p_i suggests considerably reduced miscibility. The number $M^{(i)}_{(e)}$ of end groups on a single chain of component i may be represented[30] exactly in terms of the number of tri- and tetrafunctional carbon atoms through

$$M^{(i)}_{(e)} = M^{(i)}_{(tri)} + 2M^{(i)}_{(tetra)} + 2 \tag{3.7}$$

Substituting eq 3.7 in eqs 3.3 and 3.5 converts eq 3.6 into the equivalent form

$$r = \left|\left[1 - p_1 + \frac{M^{(1)}_{(tetra)}}{M_1}\right]g_1 + 2\left(p_1 - \frac{2}{M_1}\right) - \left[1 - p_2 + \frac{M^{(2)}_{(tetra)}}{M_2}\right]g_2 - 2\left(p_2 - \frac{2}{M_2}\right)\right| \tag{3.8}$$

Equation 3.8 provides additional insight into why the rule of thumb expression $p = |p_1 - p_2|$ fails to correlate completely with the computed miscibilities of polyolefin blends. The difference in stiffness between the two blend components guarantees the presence of an additional (and perhaps larger) numerical difference between r and p, a difference that often exceeds that from the extra $M^{(i)}_{(tetra)}$ terms noted by Dudowicz and Freed previously.

We now test the new relation obtained by using eq 3.6 for the entropic structural parameter r in eq 3.1. The number of united atom groups is, therefore, again constrained to be identical for all components ($M = M_1 = M_2$), and all van der Waals energies are likewise set to be equal (using the same value $\epsilon_{ij}/k_B = 207.575$ K as Dudowicz and Freed) for the model blends considered in this subsection. (Section IV considers computations with all ϵ_{ij} unequal.) Computations are performed for all binary blends with components having the monomer structures depicted in Figure 1. In addition, for a given

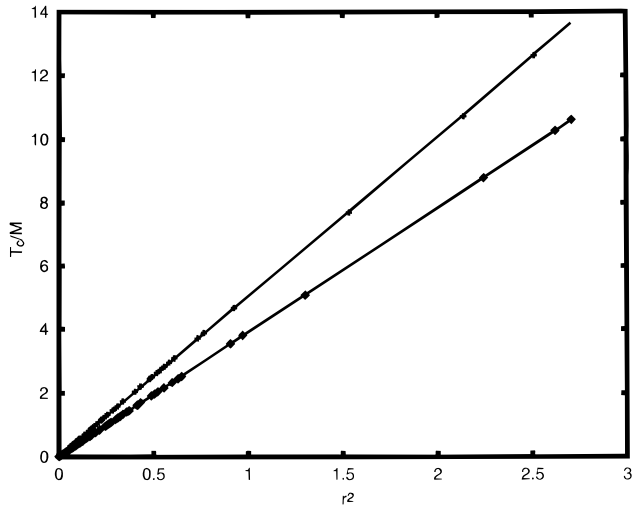

Figure 6. T_c/M as a function of the structural parameter r^2 in eq 3.7. The upper and lower curves represent the best fit of a straight line through data for $T_c = 500$ and 300 K, respectively. Similar near-perfect linear fits emerge for critical temperatures between 300 and 500 K, generating a family of curves as a function of T_c. The slopes and intercepts of these lines vary quadratically and linearly with T_c, respectively.

pair of components, the bending energies of either or both components are varied to yield "new" model blends. The number $M = M_1 = M_2$ of united atom groups is determined such that every blend has a particular critical temperature T_c. Figure 6 summarizes these 105 calculations for blends with critical temperatures T_c of either 300 or 500 K. These model blend computations produce T_c/M as varying essentially linearly with r^2 for each separate value of T_c. For example, the upper and lower curves in Figure 6 apply for $T_c = 500$ and 300 K, respectively. With the introduction of bending energies into eq 3.8, the form of eq 3.1 still correlates the computed data, provided the coefficients A and B now become functions of T_c. The variation of A and B with T_c is not evident in the work of Dudowicz and Freed because they use fewer examples. Studies of model blends with variable T_c yield the coefficients $A(T_c)$ and $B(T_c)$ as functions of T_c over the range between 300 and 500 K with the explicit representation

$$\frac{T_c}{M} = A(T_c)r^2 + B(T_c) \tag{3.9}$$

where

$$A(T_c) = -1.5396 + 0.025746T_c - 2.52 \times 10^{-5}T_c^{\,2}$$

and

$$B(T_c) = 6.318525 \times 10^{-5}T_c - 0.018205625$$

Equation 3.9 may be applied to compute M given T_c or to obtain T_c given M by an iterative solution of eq 3.9.

Equation 3.9 has several limitations. For example, eq 3.9 is fairly accurate (less than 3% error) in predicting M for a fixed T_c, except when r^2 is less than about 8×10^{-4}, where errors of closer to 20% become more common. The errors for small values of the structural parameter arise from several features. First, r is calculated using a formula for the entropic χ in the incompressible limit. The spinodals, however, are determined for a compressible blend at $P = 1$ atm, and small changes in relative volumes become significant as $N_2(1)$ and $N_2(2)$ become nearly identical numerically. Extensions of eq 3.8 to include contributions from volume changes on mixing are rather complicated and, in any circumstance, are not important since a rather small r implies a very high miscibility for blends with T_c lying between 300 and 500 K. Moreover, as noted by Dudowicz and Freed and as described in section IV, the departure of the exchange energy ϵ_{ex} from zero induces significant changes in T_c at constant M, as it does in Flory–Huggins and other theories. In addition, when the numbers of united atom groups differ for the two components, corrections to the left hand side eq 3.9 are required, as described in section IV.C.

IV. Comparison with Experiment

Reference 20 demonstrates that the LCT and PRISM theory yield nearly identical constant volume global N_c–ξ phase diagrams for corresponding semiflexible "athermal" models of polyolefin blends, even though the PRISM theory is considered by many as more realistic simply because it is an off-lattice as opposed to a lattice theory. This identity of the spinodals in the simple "athermal" limit combines with prior success of the LCT in describing many experimental data to motivate the applications presented in this subsection. Comparisons of the semiflexible chain LCT with experimental phase behavior of binary homopolymer polyolefin blends are possible by virtue of the analytical nature of the LCT free energy expressions, permitting the rapid computation of numerous constant pressure phase diagrams.

Subsections A, B, and C describe, respectively, the determination of the semiflexible chain LCT bending energies from experimental data for the mean squared radii of gyration or Kuhn lengths, the determination of the self-interaction van der Waals energies from isothermal compressibility data, and the estimation of the heteropolymer contact energies for several blends. Because experimental thermodynamic properties differ somewhat between samples due to variations in branching, microstructure, polydispersity, etc., we restrict the fitting procedure to employ data obtained only for the same samples. The limited published data for the samples of Graessley, Lohse, and co-workers imparts a measure of inaccuracy for the parameters, but these inaccuracies are not expected to be overly serious in our exploration of general trends. Subsection C contains some comparisons between the computed LCT constant pressure phase behavior and experiments. The LCT reproduces the observed experimental trends, including several enigmatic ones concerning blends containing PIB. Subsection C closes with quantitative predictions for the very interesting model P2B/PIB blends, a system studied by Dudowicz and Freed because it yields a vanishing p parameter, but a nonzero entropic structural parameter r. Since P2B has not yet been made, the LCT spinodals calculated for a range of ϵ_{ij} provide a challenge for further experimental testing of the LCT.

A. Extraction of Bending Energies from Experiment. The first serious test of the theory is whether the complex rotational isomeric states present in a real polymer chain in the melt can be represented adequately by the lattice model with just two local states, trans and gauche, and with the same bending energies for pairs of backbone and side chain gauche bonds on the same chain (an assumption applied here solely to minimize the number of adjustable parameters since theory can easily be applied with different E_b for backbone and side group bends). Dividing the approximate expression in eq 2.14 for the mean squared

radius of gyration $\langle R_G^2 \rangle$ by the molecular weight yields effectively a function only of the bending energy at fixed temperature. Thus, experimental data for $\langle R_G^2 \rangle$ enable the determination of E_b. We begin the evaluation of the LCT model parameters with the head-to-head polypropylene (hhPP) melt because this sytem is a "pure" homopolymer that is uncomplicated by the microstructural randomness which, for example, plagues diene-based syntheses and can grossly affect phase behavior.[31] Graessley and co-workers[5] extract the radius of gyration of hhPP from small angle neutron scattering for three different molecular weight hhPP/D−hhPP blends (where D refers to the deuterated form). Calculating the bending energy from the experimental $\langle R_G^2 \rangle$ for each of the three molecular weights at 300 K yields the average bending energy E_b(hhPP) = 276.934 K, with an average deviation in E_b of about 5.5 K (a 2% error), which is well within the experimental error of nearly 5% for $\langle R_G^2 \rangle$.

Encouraged by the successful LCT fit to data for $\langle R_G^2 \rangle$ of hhPP, we now determine bending energies for the other polymers in Figure 1 based on less extensive information. The data of Graessley and co-workers[5] (Table 3 of ref 5) for PP (with polymerization index 705) yield the bending energy E_b(PP) = 219.340 K, while data for PIB (from Flory[32]) produce E_b(PIB) = 312.871 K. The PEP data from Table 8 of Graessley and co-workers[5] are presented in terms of statistical segment lengths, a, which, in turn, are represented in terms of the radius of gyration through

$$a = \sqrt{\frac{6 v_{ref} {R_G}^2}{N v(T)}} \tag{3.10}$$

where the reference volume v_{ref} is a constant (=100 Å^3), N is the polymerization index, and the monomer volume $v(T)$ for the component is a weakly varying function of temperature. Because the functions $v(T)$ are not provided, the extraction of $\langle R_G^2 \rangle$ from the data proceeds with the following analysis: Taking the ratio of eq 3.10 for the statistical segment lengths of two different polymers leads to a cancellation of the reference volumes. If the monomer species have very similar structures, the volumes $v_i(T)$ are expected to be nearly identical, yielding a rough cancellation of the monomer volumes in the ratio a_1/a_2. This approximation produces the ratio of the statistical segment lengths as

$$\frac{a_1}{a_2} = \sqrt{\frac{{R_{G,1}}^2 N_2}{{R_{G,2}}^2 N_1}} \tag{3.11}$$

Tables 3 and 8 of Graessley *et al.*[5] contain data both for the $R_{G,i}$ and a_i of hhPP, PP, and PEP. Hence, eq 3.11 may be tested for these cases, and this approximation is correct to within 1% when a_1 and a_2 are the statistical segment lengths for hhPP and PP. Similarly, when a_1 is the experimental statistical segment length for PEP, eq 3.11 produces nearly identical PEP radii of gyration with a_2 being either the experimental statistical segment length for hhPP or for PP. Thus, this radius of gyration is inserted into eq 2.14 to produce the bending energy E_b(PEP) = 460.602 K.

Since data for $\langle R_G^2 \rangle$ or a are not available from Graessley *et al.* for the PE samples they study and since use of data for other samples produces considerable uncertainties due to sample variations, an alternative method for estimating E_b(PE) proceeds as follows: The PEP polymer is an alternating copolymer of ethylene and propylene, so the above single bending energy E_b(PEP) is in reality some (complex) average of the bending energies for PE and PP. Rather than developing a more complicated expression with two (or more) bending energies, we employ the simplest *ad hoc* model in which E_b(PEP) is taken as the mean of the bending energies for its two alternating species

$$E_b(\mathrm{PEP}) = \frac{E_b(\mathrm{PE}) + E_b(\mathrm{PP})}{2} \tag{3.12}$$

This simple model suffices for the purposes of describing qualitative trends. Equation 3.12 enables E_b(PE) to be determined from the above values of E_b for PP and PEP as E_b(PE) = 263.284 K. Since the monomer structure of hhPP is identical to that of the alternating polymer poly(ethylene 2-butene), applying a similar model to eq 3.12 yields E_b(P2B) = 290.585 K as the required final bending energy. A rough determination of E_b(P2B) is useful for the predictions in Subsection D since P2B has, to our knowledge, not been studied experimentally.

Work in progress by Dudowicz and Freed combines the above determined bending energies with the correlation in eq 3.6 to provide a microscopic molecular explanation for the observation[4] that hhPP mixes more favorably with PEP than PP.

B. Extraction of Self-Interaction van der Waals Energies from Experiment. The self-interaction energies ϵ_{ii} are calculated for each polymer species from the isothermal compressibility data of Lohse, Graessley, and co-workers[33] for polyolefin homopolymer melts. The data are presented only as averages taken over a range of pressures from 10 to 40 MPa for a series of temperatures and for samples with molecular weights large enough "to ensure that the *PVT* properties depend only on the chemical microstructure of the polymer."[33] The average nature of this data is yet another feature dictating a consideration of only basic trends. In order to fit ϵ_{ii} to the data, for convenience, the pressure is taken as the average of 25 MPa, and the relevant molecular weights are fixed as the values presented in other papers by the same authors.[4,5] The individual self-interaction van der Waals energies ϵ_{ii} are calculated from a least squares fit of the LCT isothermal compressibility of eq 2.6 to the experimental data. Although the least-squares fit of the isothermal compressibility data is not strongly affected by small changes in the large molecular weights, the fitted homopolymer contact energy ϵ_{ii} diminishes on the order of 0.05 K when determined for a sample with double the molecular weight. Since the exchange energy ϵ_{ex} is a small difference between large numbers, the uncertainties in previous analyses of the experimental data and the distributions of molecular weights may produce a rather large percentage changes in ϵ_{ex}, again restricting our attention to qualitative trends. In addition, fitting the ϵ_{ii} to the isothermal compressibility data, obtained by specifying the pressures as 10 or 40 MPa, shifts the ϵ_{ii} by ±5−7%, a variation with an even larger impact on ϵ_{ex}.

The homopolymer contact energies ϵ_{ii} are determined as 234.46, 202.19, 207.49, 222.53, and 208.60 K for PE, PP, PEP, PIB, and hhPP, respectively. Subsection D considers a range of ϵ_{ii} for P2B and the resulting influence on the miscibility of a P2B/PIB blend. The homopolymer van der Waals energy for PE is very likely incorrect since only one high temperature data point is available for the isothermal compressibility. Hence, no phase diagrams are calculated for blends involving PE.

C. Extraction of Interaction Energies ϵ_{12} from Experiment and Comparisons of Phase Behavior with Experiment. The only remaining quantities needed for calculating the binary blend phase diagram are the heteropolymer van der Waals energies ϵ_{12}, which are determined by adjusting ϵ_{12} such that the experimental and theoretical critical temperatures T_c and compositions Φ_c agree for two blends with the same components but different molecular weights. The ϵ_{12} for several of the blends considered below may be varied only on the order of 0.05 K and still yield quantitative agreement with experimental phase boundaries. An alternative determination of ϵ_{12} proceeds by fitting experimental small angle neutron scattering (SANS) intensities or the SANS Flory χ parameters to the appropriate theoretical expressions, as has been done previously.[34] We chose to determine ϵ_{12} from the T_c and Φ_c for two samples (when available) and then to check whether using this choice in the LCT produces the correct qualitative behavior for other samples studied experimentally.

For example, experiments for PEP/hhPP ($M_1 = 4276$; $M_2 = 1921$, 5461, or 12271) blends exhibit an upper critical solution temperature (UCST). The curved variation of the SANS Flory χ parameter with inverse temperature also suggests the possible (but unobserved) presence of a lower critical solution temperature (LCST).[5] Fitting the LCT parameter ϵ_{12} to the UCST blend critical properties yields the heterocontact energy $\epsilon_{12} = 208.13$ K, which translates into $\epsilon_{ex} \approx -0.4$ K for this blend. The LCT phase diagrams calculated using this set of ϵ_{ij} only display an upper critical temperature. At higher pressures and for a wide range of different polymerization indices, the LCT computations for PEP/hhPP blends produce only a UCST transition, with increasing pressure enhancing blend miscibility. At elevated temperatures, the model system approaches but does not reach phase separation (a readily testable suggestion.)

In contrast, the PEP/PP blend is observed[5] to be completely miscible over the temperature range $300 \leq T \leq 430$ K, allowing us only to determine a minimum heteropolymer van der Waals energy ϵ_{12} such that this blend does *not* have spinodals within this temperature range. The minimum calculated ϵ_{12} for the PEP/PP ($M_1 = 4276$, $M_2 = 781$) blend is $\epsilon_{12} = 204.78$ K, which yields the slightly positive exchange energy of $\epsilon_{ex} = 0.12$ K for this blend. This minimum acceptable value for ϵ_{12} is probably more reasonable since it produces a computed critical temperature near 300 K (agreeing with a suggestion in the footnotes to Table 4 of Graessley *et al.*[5]), but not in the temperature range $300 \leq T \leq 430$ K for which data are given. Figure 7 displays the theoretical spinodal for a PEP/PP ($M_1 = 4276$; $M_2 = 781$) blend at a pressure of $P = 1$ atm. This blend is observed to be miscible experimentally for the temperature range 300 K $\leq T \leq$ 430 K. The SANS χ parameter is a nonlinear function of $1/T$ with a negative curvature,[5] suggesting the possibility of an LCST at higher temperatures. The LCT computations in Figure 7 clearly predict both LCST and UCST phase transitions, but the LCST lies above the decomposition temperature. Calculated phase diagrams for different $\{M_i\}$ suggest that the LCST does not change significantly with molecular weights, while the UCST varies sensitively with changes in the $\{M_i\}$. The LCT computations predict only a UCST (not an LCST) in the temperature range 300 K $\leq T \leq$ 430 K when the PP polymerization index lies between 375 and 525 while the PEP polymerization index is fixed at 855. For the above temperature range, complete miscibility is computed for PP polymerization indices below 375, while little miscibility appears for PP indices above 525.

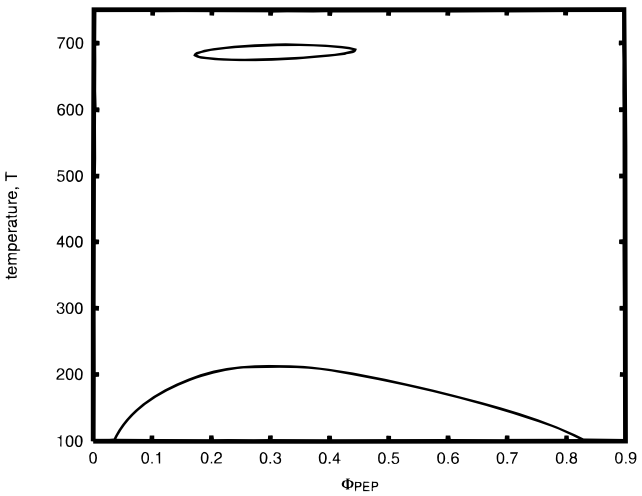

Figure 7. Constant pressure ($P = 1$ atm) $T - \Phi$ spinodal for a PEP/PP blend. The bending energies, van der Waals energies, and polymerization indices are E_b(PEP) = 460.602 K, E_b(PP) = 219.34 K, $\epsilon_{PEP,PEP} = 207.49$ K, $\epsilon_{PEP,PP} = 204.78$ K, $\epsilon_{PP,PP} = 202.19$ K, $N_{PEP} = 855$, and $N_{PP} = 260$. The spinodal has two branches, indicating the presence of both an upper (UCST) and a lower (LCST) critical solution temperature. The LCST changes marginally with large modifications in pressure or in polymerization indices, whereas the UCST is extremely sensitive to such variations.

The hhPP/PP ($M_1 = 1921$; $M_2 = 781$) blend exhibits UCST behavior experimentally, but insufficient data are available to compute the heteropolymer van der Waals energy. The critical temperature−composition phase diagram is not determined experimentally but is presumed to lie below 300 K. If ϵ_{12} is chosen to produce a vanishing exchange energy ($\epsilon_{ex} = 0$ K), LCT computations for this model blend yield a UCST at 290 K. This UCST is virtually insensitive to pressure, with T_c increasing by about 3 K as the pressure is raised from 1 to 1000 atm. Allowing the exchange energy to be slightly negative ($\epsilon_{ex} = -0.05$ K) produces complete miscibility between 100 and 1000 K for pressures between 1 and 10^4 atm.

The near zero exchange energy that likely applies to the hhPP/PP ($M_1 = 1921$; $M_2 = 781$) blend enables another comparison between the "experimental" and predicted critical temperatures using the remarkable correlation in eq 3.9 which is based on $\epsilon_{ex} = 0$. Since eq 3.9 applies for $M_1 = M_2$, a condition not satisfied for this hhPP/PP blend, we now extend this correlation to $M_1 \neq M_2$. Application of the stability condition to incompressible Flory−Huggins theory yields the critical temperature scaling with M_1 and M_2 as

$$T_c \sim \frac{4M_1M_2}{[\sqrt{M_1} + \sqrt{M_2}]^2} \equiv M_{eff} \qquad (3.13)$$

Since the left hand side of eq 3.9 contains T_c/M, a reasonable extension to unequal $\{M_i\}$ ($M_1 \neq M_2$) replaces T_c/M by T_c/M_{eff}. When the effective number M_{eff} of united atom groups for the hhPP/PP ($M_1 = 1921$; $M_2 = 781$) blend is chosen according to eq 3.13, then eq 3.9 yields an identical critical temperature ($T_c \approx 294$ K) to that calculated from the full LCT spinodal calculation. Computations for several other blends (including ones in which neither component is hhPP or PP) yield agreements similar to those found for the PP/hhPP blend when M_{eff} replaces M in eq 3.9 and when all van der Waals energies are equal (with $\epsilon_{ij} = 207.575$ K).

While eq 3.9 with the substitution $M \rightarrow M_{eff}$ has been tested for fewer cases than eq 3.9, the new correlation with M_{eff} replacing M further greatly extends the applicability of eq 3.9. Nevertheless, eq 3.9 still applies within the equal ϵ model and requires extensions to describe the dependence on the exchange energy.

The PIB-containing blends display considerably different phase behavior from the other polyolefin blends studied by Graessley, Lohse, and co-workers. These blends yield mostly negative, occasionally large interaction parameters χ^{SANS}, and only LCST behavior is observed experimentally. The fit of the LCT to experimental critical properties produces a large, negative exchange energy for the PIB/PEP ($\epsilon_{ex} = -2.2$ K) blends and for the PIB/hhPP ($\epsilon_{ex} = -1.3$ K) blends listed in Table 2 of Krishnamoorti *et al.*[4] We note that, unlike the agreement between theory and experiment found for the other blends considered here, the LCT computations with an exchange energy of −1.3 K for the PIB/hhPP blends produce phase diagrams that just barely lie within the published experimental error ranges (see below) because the phase diagrams are very sensitive to changes in ϵ_{ex}. The PIB/hhPP ($M_1 = 5841$; $M_2 = 1921$) and PIB/hhPP ($M_1 = 11441$; $M_2 = 12271$) blends exhibit experimental critical temperatures between, respectively, 175 and 200 °C and between 165 and 185 °C, while the corresponding theoretical critical temperatures are 196 and 166 °C, respectively. The exchange energy for the PIB/PP blend can not be determined due to insufficient data, but the exchange energy for PIB/PP is more positive ($\epsilon_{ex} > -2.2$ K) than that for the PIB/PEP blend since the computed critical temperature would lie in the experimental temperature range ($300 \leq T \leq 430$ K) when $\epsilon_{ex} = -2.2$ K is used with the PIB/PP blend. The exchange energies for these three blends suggests that a less negative exchange energy emerges when PIB is blended with a component having an increasing average number of methyl (CH_3) groups per backbone atom. No similar trend is present in the heteropolymer contact energies, which are roughly the same within experimental uncertainties.

Graessley and co-workers[4] expressed surprise in finding that the critical temperature hardly varies when the molecular weights of the components in the PIB containing blends are changed by an order of magnitude. The LCT computations also reveal that the critical temperatures for the PIB blends should be fairly insensitive to changes in molecular weight. This absence of a molecular weight dependence arises in the LCT computations from the large, negative exchange energies combined with the presence of the noncombinatorial entropy that appears by virtue of treating chains of structured monomers. This common feature of LCT predictions for LCST type blends is readily illustrated for the $P \rightarrow \infty$ limit where the $\Phi = {}^1/_2$ spinodal condition takes the form $(A - B/T_s)N = 2$, where B is positive for systems with negative exchange energies ϵ_{ex} and where the noncombinatorial entropy A is generally positive. Solving for T_s yields $T_s = BN/(AN - 2)$ which approaches the constant N-independent limit of $T_s = B/A$ for $AN >> 1$ and for being N the polymeration index. Although the critical composition generally departs from $\Phi = 0.5$, both the critical temperature T_c and T_s scale similarly with N. LCT computations also indicate that elevating the pressure increases the blend miscibility for each of the three PIB blends considered here. These comparisons with experiment demonstrate that the LCT provides physical insights into the qualitative phase behavior of polyolefin blends. The LCT model is quick, yet effective, to apply, with the major limitation being the need for more empirical data than for application of simple incompressible FH theory.

In order to illustrate further the use of the LCT to predict the phase behavior of binary polyolefin blends, we close this section by determining the temperature-composition phase diagrams for two PIB/P2B blends ($M_{PIB} = 5841$, $M_{P2B} = 402$ or 4002). Since ϵ_{22} is unknown for P2B, we calculate LCT phase diagrams using three different P2B self-interaction energies, $\epsilon_{22} = 222.53$ (same as PIB), 234.46, and 201.34 K. For each ϵ_{22}, phase diagrams are determined for exchange energies of 0 and ±0.5 K, yielding a total of 18 separate phase diagrams for the two blends. We restrict attention to the physically more interesting temperature region between 300 and 470 K. All the model blends with positive exchange energies are nearly completely immiscible over the entire composition range, with a UCST well above 500 K. In contrast, all the model PIB/P2B blends with the negative exchange energy ($\epsilon_{ex} = -0.5$ K) are completely miscible, except for $\epsilon_{22} = 201.34$ K where an LCST occurs at 350 and 440 K for the blend with the P2B component having $M_{P2B} = 4002$ and 402, respectively. When the exchange energy vanishes, the blends with $M_{P2B} = 4002$ are always immiscible, while the blends with $M_{P2B} = 402$ are miscible, except when $\epsilon_{22} = 201.34$ K (where complete immiscibility in the temperature range is present). These predictions are fairly easy to test once P2B is synthesized.

V. Discussion

The generalization of the lattice cluster theory (LCT) to semiflexible chains is used for testing the fundamental assumptions invoked by several prior models of binary blend miscibility. The possibility of fabricating carefully controlled polyolefins allows detailed comparisons between LCT computations and a growing number of experiments for polyolefin blends. The present comparisons for binary blends illustrate the power of the theory and the methods for its application.

The semiflexible LCT model provides an excellent vehicle for our tests here of the importance of some assumptions previously invoked to explain aspects of polyolefin miscibilities. For example, the remarkable correlation of Dudowicz and Freed[18,19] demonstrates that blend miscibility is sensitive to molecular structure as well as to the energetic interactions, while the LCT computations in ref 20 support prior contentions that chain semiflexibility strongly influences phase behavior. The semiflexible LCT model simultaneously incorporates monomer structure, trans−gauche bending energies, van der Waals interactions, and compressibility. A model of this complexity should begin to mimic the behavior of real polymer blends.

One prior theory of polyolefin miscibilities is based on solubility parameter theory[2−7] has been used to argue that only enthalpic differences are required to explain most of the observed miscibility patterns for polyolefin blends. Although solubility parameter theory describes most of the polyolefin data, this simple model cannot predict the miscibilities of blends that exhibit lower critical solution temperatures. Therefore, *ad hoc* treatments of lower critical solution temperature (LCST) blends have been employed since the solubility parameter theory provides no insight into the microscopic behavior of the blend. Consequently, our comparisons with experiment explicitly consider examples (blends containing PIB) for which the solubility parameter theory fails completely. These examples are important because remedying the failures of a theory provides one

sure route toward developing deeper understanding of the underlying physics.

At the other extreme, Bates, Fredrickson, and co-workers[8−12] (BF) append Gaussian fluctuations to incompressible Flory−Huggins (FH) theory for athermal chains (i.e., chains with a vanishing Flory interaction parameter χ) to predict that differences in stiffness between the two components alone determine polymer miscibility. We first test the implication of the BF theory that complete miscibility would arise for a blend with a vanishing stiffness disparity ξ. This test employs LCT computations of the phase behavior for binary blends of a semiflexible linear chain with several other united atom model polyolefins, whose monomers are exhibited in Figure 1. These phase behaviors are summarized using a global phase diagram that depicts the minimum number M_c of united atom groups necessary to produce phase separation as a function of the stiffness disparity ξ. The inclusion of chains with specific monomer structures requires the highly nontrivial development of (approximate) expressions for the mean squared radius of gyration $\langle R_G^2 \rangle$ of a nonreversing random walk in order to evaluate ξ. The BF model would predict that M_c diverges as ξ vanishes, but Figure 4 demostrates that no such divergence occurs for the LCT computations and that the highest miscibility emerges for more negative ξ (corresponding to large negative bending energies). We also consider ξ for a short-range self-avoiding walk to determine if the use of a different chain statistics supports the BF theory, which implies that vanishing ξ produces enhanced miscibility. This change in chain statistics, however, leaves the global phase diagrams basically unchanged. The LCT computations support the contention that stiffness differences influence miscibility, but complete miscibility does not ensue with vanishing ξ. Thus, stiffness disparity cannot be the only factor driving polyolefin phase behavior. On the other hand, some blends with equal polymerization indices become completely miscible below some bending energy threshhold, suggesting that appropriate asymmetric combinations of both polymerization indices and bending energies may produce miscible blends.

LCT computations for binary blends involving a semiflexible linear chain and a corresponding structured monomer chain serve as an excellent test of the accuracy of the thermodynamically equivalent chain model of Schweizer and co-workers. Although we are currently unable to evaluate complete pair distribution functions within the LCT, the parameter ξ is represented only in terms of intramolecular properties, and some ξ should coincide with the case where the model and real chains have the most similar intramolecular pair correlation functions. Consequently, we provide LCT computations for binary blends with one semiflexible linear chain and another structured monomer chain as a function of the bending energy of the former to cover all possible cases. Since no bending energy in Figure 4 is sufficient to produce complete miscibility, the effective semiflexible linear chain should have other features altered, including bead sizes (which need not all be identical), bond lengths, numbers of beads in the linear chain, etc., in order to achieve an optimal thermodynamic match.

We significantly extend the remarkable correlation, eq 3.1, of Dudowicz and Freed[18,19] (which correlates T_c/M with the square of the entropic structural parameter r^2) to include the influence of chain semiflexibility and to cover unequal numbers ($M_1 \neq M_2$) of united atom groups. The new correlation retains the form $T_c/M_{eff} = Ar^2 + B$, with $M_{eff} = 4M_1M_2/[\sqrt{M_1} + \sqrt{M_2}]^2$ and with r now dependent on the bending energies in addition to the fractions of tri- and tetrafunctional carbons in the chain. The coefficients A and B are, respectively, quadratic and linear functions of the critical temperature, and the correlation is still restricted to the simplified model in which all polyolefin united atom groups interact with a common single interaction energy. Equation 3.8 reproduces the full LCT computations extremely accurately (<3% error) for blends with T_c lying in the temperature range between 300 and 500 K and for r^2 greater than about 8×10^{-4}.

Equation 3.8 still posesses several limitations. Other physical factors predominate the determination of T_c in the most miscible systems with $0 \approx r^2 < 8 \times 10^{-4}$, but these errors are, perhaps, not too serious because of the high miscibility. The expression used for r is derived from the incompressible limit of the LCT noncombinatorial entropy, but the LCT critical temperatures are computed for a compressible system at a constant pressure of 1 atm, which is considerably less than the 10^5 or 10^6 atm necessary to approach incompressible conditions. All experimental polymer blends are well known to be compressible as evidenced by their nontrivial equations of state and volume changes upon mixing. The most important influence of compressibility on the phase behavior does not emerge from the "equation of state effects" arising from small volume changes on mixing. Instead, a compressible binary blend contains, *at minimum*, three independent van der Waals energies whose disparities exert a significant influence on the blend phase behavior,[20,34−36] especially for structured monomer models where energetic asymmetries may appear even when both components have nearly equal melt densities. Simple models with monomers occuping single lattice sites yield pure melts whose densities vary proportionally with differences in self-interaction energies ϵ_{ii}. The introduction of structured monomers alters the density of an otherwise identical melt, enabling components differing in both ϵ_{ii} and structure to exhibit the same melt densities. This dependence of the LCT (and other compressible theories) on three independent energies differs greatly from incompressible models, such as FH theory, which require that all excess thermodynamic properties be a function only of a single interaction parameter, the exchange energy ϵ_{ex} of eq 1.1. LCT calculations by Dudowicz and Freed, as well as those in ref 20 and the present work, exhibit a strong dependence of the critical temperature on the exchange energy and a lesser dependence on differences between the van der Waals energies. The correlation between r^2 and T_c/M_{eff}, however, applies only for a model of equal van der Waals energies for all species. Thus, it is desirable to extend this correlation to describe the variations of T_c with the three van der Waals energies and, perhaps, even the volume changes in mixing. Unfortunately, this extension is highly nontrivial.

The strong sensitivity of phase behavior to the exchange energy ϵ_{ex} (or its equivalent) in *all* theories of blend miscibility and the fact that ϵ_{ex} is roughly two orders of magnitude smaller than the individual homopolymer ϵ_{ii} and heteropolymer ϵ_{ij} van der Waals energies strongly suggest that these energies must be obtained semiempirically from some experimental properties. Our comparisons of LCT computations with experimental data for polyolefin blends illustrate the types of experimental data that may be used to specify the LCT interaction parameters. For example, the

bending energies and homopolymer contact energies are extracted here from homopolymer melt experimental data for the radius of gyration and isothermal compressibility, respectively. The heteropolymer van der Waals energy ϵ_{12} can be determined directly from small-angle neutron scattering intensities or critical properties, and the latter method is applied here for several polyolefin blends.

Comparisons between experimental data and our theoretical description of $\langle R_G^2 \rangle$ for semiflexible, structured monomer lattice chains indicate the accuracy of the lattice model with explicitly included trans and gauche states but one bending energy to represent the complex rotational energy states present in a real polymer chain. These results suggest that a single bending energy for backbone and side group gauche configurations suffices for describing the polyolefin chain stiffnesses.

LCT computations have been performed for many model binary polyolefin blends with semiflexibility introduced through the added bending energies. Depending on the energetic parameters, the blends display either an LCST or a UCST in the experimentally accessible range (between glass transition and decomposition temperatures), but usually not both types of transitions. For example, the experimental SANS Flory χ parameters for blends of PEP with either PP or hhPP vary nonlinearly with inverse temperature, indicating that both a UCST and an LCST are possible. Our LCT calculations suggest that the LCST lies above a decomposition temperature for these two systems. Furthermore, the sign of the exchange energy ϵ_{ex} *does not* always correlate with the type of critical solution temperature appearing in the desired temperature range. For example, the fit of energetic parameters to the LCT yields a modestly negative exchange energy ($\epsilon_{ex} \approx -0.4$ K) for PEP/hhPP blends, yet LCT computations only produce a UCST, presumably due to the presence of the noncombinatorial entropy.

Blends formed from PIB and other polyolefins are of extreme interest since they lead to LCST phase diagrams that cannot be explained within a pure solubility parameter theory. Furthermore, experiments for these systems exhibit a perplexing absence of a dependence of T_c on molecular weights.[4] The fit of the LCT to experiment for PIB-containing blends yields rather large and negative exchange energies ($\epsilon_{ex} = -2.2$ and -1.3 K for PIB/PEP and PIB/hhPP blends, repectively.). The enormous magnitude of the exchange energy in these blends explains why LCT computations and experiment alike find only small changes in the critical temperature from modifying polymerization indices by more than an order of magnitude, a feature explained within the LCT by the presence of the noncombinatorial entropy. Because P2B has not yet been made, calculations are also performed for PIB/P2B blends with a range of ϵ_{ij}. This set of predictions, therefore, provides a challenge for testing the LCT further.

Acknowledgment. We thank Jacek Dudowicz, Mary Jay, Isaac Sanchez, Ken Schweizer, and Jack Douglas for many helpful comments on the text. We thank David Lohse for discussions regarding his data. This research is supported, in part, by Grant No. DAAG55-97-1-0162 from the ARO.

Appendix A

We illustrate the calculation of the first few terms in eq 2.14 for $\langle R_G^2 \rangle$ using the lattice model for polypropylene (PP). All possible contributing averages $W_{n+1,s}(\alpha,\beta)$ and their counting factors $N_{n+1,s}(\alpha,\beta)$, necessary for constructing the expression for $\langle R_G^2 \rangle$ (eq 2.14), are then tabulated (Table 1) for the polymers represented in Figure 1. The calculations apply to both nonreversing random walk (NRRW) and short-range self-avoiding walk (SAW) models.

Calculating the averages $W_{n+1,s}(\alpha,\beta)$ in eq 2.14 is fairly straightforward for Gaussian linear chains and is described in ref 20. Branched chains have side groups whose placement on the lattice affects the sites available for positioning other bonds. Thus, determining the averages $W_{n+1,s}(\alpha,\beta)$ for branched chains is complicated by a need to consider the number of configurations available to the side groups for a given backbone configuration and by the additional excluded volume constraints imposed by the presence of side groups. We now focus on the unique structures obtained from a PP chain for a connecting path length of two bonds (Figure 3a).

The PP chain yields only two possible unique topologies (structures 1 and 2 in Figure 3a) for a path length of two bonds. Structure 1 in Figure 3a has only one pair of bonds and hence one contributing average, while structure 2 in Figure 3a has two qualitatively different possible pairs of bonds that may be selected from the three bonds in the structure: backbone−backbone and backbone−side chain pairs of bonds. Therefore, the PP structure produces $T_1 = 2$ unique structures for averages of pairs of consecutive bonds, with the second unique structure contributing two different types of correlations [(b,b) and (b,s) bond pairs]. The average correlation $W_{2,s}(\alpha,\beta)$ between each of these pairs of bonds can be computed for any model, but explicit calculations are now provided using the NRRW and short-range SAW models.

The average $W_{2,1}$(b,b) for the backbone-backbone pair in structure 1 of Figure 3a is trivially obtained by first noting that a collinear conformation of the two bonds produces the only nonzero contribution from the Kronecker deltas in eq 2.13 for both the NRRW and the SAW models. The total number of configurations possible for structure 1 of Figure 3a is the collinear configuration plus all $z - 2$ bent conformations. Each bent configuration incurs an energy penalty $\exp(-E_b/k_BT)$, leading to the thermal average of z_{b1} total configurations, where z_{b1} is related to the z_b in eq 2.1 as

$$z_{bx} = z_b - x \exp(-E_b/k_BT) = 1 + (z - 1 - x) \exp(-E_b/k_BT) \quad \text{(A.1)}$$

with $x = 1$. Thus, the nonzero contribution to $W_{2,1}$(b,b) emerges from the one collinear configuration out of the z_{b1} total possible configurations of the unique structure 1 in Figure 3a for both the NRRW and the SAW models, thereby yielding $W_{2,1}(b,b) = 1/z_{b1}$ in Table 2.

The average $W_{2,2}$(b,b) for the backbone-backbone pair in unique structure 2 of Figure 3a is calculated differently from the average $W_{2,1}$, since the definition of a NRRW must be generalized for branched structures. A branched NRRW is defined to be a walk whose only restriction is the self-avoidance of the two terminal monomers on a pair of consecutive bonds. Equivalently, all nonreversing bonds are prohibited from overlapping with another bond that shares a common monomer. As in the calculation of $W_{2,1}$(b,b), only the collinear configuration of the backbone bonds contributes to the average in eq 2.14. When the backbone bonds are fixed in a collinear configuration, the side chain bond has $z - 2$

Table 2. Average Correlations $W_{n+1,s}$ for Local Structures with Connecting Paths of up to Four Bonds[a]

	NRRW	SAW
$W_{2,1}$(b,b)	$1/z_{b1}$	$1/z_{b1}$
$W_{2,2}$(b,b)	$1/z_{b1}$	$1/z_{b1}$
$W_{2,2}$(b,s)	E/z_{b1}	E/z_{b1}
$W_{2,3}$(b,b)	$z_{b3}/[z_{b3}z_{b1} - 2E(1 - E)]$	$z_{b3}/[z_{b3}z_{b1} - 2E(1 - E)]$
$W_{2,3}$(b,s)	$(z - 3)E^2/[z_{b3}z_{b1} - 2E(1 - E)]$	$(z - 3)E^2/[z_{b3}z_{b1} - 2E(1 - E)]$
$W_{2,3}$(s,s)	$z_{b3}/[z_{b3}z_{b1} - 2E(1 - E)]$	$z_{b3}/[z_{b3}z_{b1} - 2E(1 - E)]$
$W_{3,1}$(b,b)	$1/z_{b1}^2$	$1/z_{b1}^2$
$W_{3,2}$(b,b)	$1/z_{b1}^2$	$1/z_{b1}^2$
$W_{3,2}$(b,s)	E/z_{b1}^2	E/z_{b1}^2
$W_{3,3}$(b,b)	$1/z_{b1}^2$	$1/z_{b1}^2$
$W_{3,3}$(b,s)	E/z_{b1}^2	E/z_{b1}^2
$W_{3,3}$(s,s)	E^2/z_{b1}^2	E^2/z_{b1}^2
$W_{3,4}$(b,b)	$z_{b3}/[z_{b1}[z_{b3}z_{b1} - 2(1 - E)E]]$	$z_{b3}/[z_{b1}[z_{b3}z_{b1} - 2(1 - E)E]]$
$W_{3,4}$(b,s)	$(z - 3)E^2/[z_{b1}[z_{b3}z_{b1} - 2(1 - E)E]]$	$(z - 3)E^2/z_{b1}[z_{b3}z_{b1} - 2(1 - E)E]]$
$W_{4,1}$(b,b)	$1/z_{b1}^3$	$1/[z_{b1}^3 - (z - 2)E^3]$
$W_{4,2}$(b,b)	$1/z_{b1}^3$	$[1 + E^2]/[z_{b1}^3 - [1 + (2z - 5)E]E^2]$
$W_{4,2}$(b,s)	E/z_{b1}^3	$E(1 + E^2)/[z_{b1}^3 - [1 + (2z - 5)E]E^2]$
$W_{4,3}$(b,b)	$1/z_{b1}^3$	$1/[z_{b1}^3 - (z - 2)E^3]$
$W_{4,4}$(b,b)	$1/z_{b1}^3$	$[(z - 2) + 2E^2(z - 3)]/[(z - 2)z_{b1}^3 - [1 + (2z - 5)E]^2E]$
$W_{4,4}$(b,s)	E/z_{b1}^3	$E[z - 1 + (z - 4)E + (z - 3)E^2]/[(z - 2)z_{b1}^3 - [1 + (2z - 5)E]^2E]$
$W_{4,4}$(s,s)	E^2/z_{b1}^3	$E^2[z + 2(z - 4)E]/[(z - 2)z_{b1}^3 - [1 + (2z - 5)E]^2E]$
$W_{4,5}$(b,b)	$1/z_{b1}^3$	$[1 + E^2]/[z_{b1}^3 - [1 + (2z - 5)E]E^2]$
$W_{4,5}$(b,s)	E/z_{b1}^3	$E(1 + E^2)/[z_{b1}^3 - [1 + (2z - 5)E]E^2]$
$W_{4,6}$(b,b)	$1/z_{b1}^3$	$[(z - 2) + 2E^2(z - 3)]/[(z - 2)z_{b1}^3 - [1 + (2z - 5)E]^2E]$
$W_{4,6}$(b,s)	E/z_{b1}^3	$E[z - 1 + (z - 4)E + (z - 3)E^2]/[(z - 2)z_{b1}^3 - [1 + (2z - 5)E]^2E]$
$W_{4,6}$(s,s)	E^2/z_{b1}^3	$E^2[z + 2(z - 4)E]/[(z - 2)z_{b1}^3 - [1 + (2z - 5)E]^2E]$
$W_{4,7}$(b,b)	$z_{b3}/[z_{b1}^2[z_{b3}z_{b1} - 2(1 - E)E]]$	$z_{b3}/[z_{b3}z_{b1}^3 - [(z - 2)z_{b3} - 2 + 2E]E^3 - 2(1 - E)Ez_{b1}^2]$
$W_{4,8}$(b,b)	$z_{b3}^2/[z_{b1}[z_{b3}z_{b1} - 2(1 - E)E]^2]$	$z_{b3}^2[z - 2 + 4(z - 4)E^2]/W^b$
$W_{4,8}$(b,s)	$(z - 3)E^2z_{b3}/[z_{b1}[z_{b3}z_{b1} - 2(1 - E)E]^2]$	$(z - 3)E^2\{(z - 2)z_{b3} + 2[(z - 3)^2E - 1]\}/W^b$
$W_{4,8}$(s,s)	$(z - 3)^2E^4/[z_{b1}[z_{b3}z_{b1} - 2(1 - E)E]^2]$	$(z - 3)E^3[z - 2 + 4(z - 4)z_{b3}E]/W^b$

[a] $E \equiv \exp(-E_b/k_BT)$ and $W^b = (z - 2)z_{b3}^2[z_{b1}^3 - (z - 2)E^3] - 4E\{z_{b3}(z - 1 - 2E) + E[(2z - 5)z_{b3}^2 + 2z(z - 4)(1 - E)z_{b3} - (1 - E)^2(z - 2)] + E^2[(1 - E)z_{b3}(z^3 - 6z^2 + 4z + 12) + z_{b3}^2(z - 3)(2z - 5) - (1 - E)^2(z^2 - z - 10)]\}$.

possible conformations for both the SAW and the NRRW models. The total number of configurations for the three bonds of the unique structure 2 of Figure 3a is $z - 2)z_{b1}$ for both the SAW and the NRRW models since each of the allowed backbone bond conformations can be combined with the same number $(z - 2)$ of side chain conformations. Hence, there are $z - 2$ placements of the side group bond that still permit a collinear configuration for the backbone bonds, thereby producing the average contribution $W_{2,2}$(b,b) for both the SAW and the NRRW models as $(z - 2)/z_{b1}(z - 2) = 1/z_{b1}$ (see Table 2).

The calculation of $W_{2,2}$(b,s) follows the same pattern as for $W_{2,2}$(b,b). Only the collinear side chain bond−backbone bond configuration contributes to the average, leaving one backbone bond free to sample all possible allowed configurations. For both types of walks, this backbone bond has $z - 2$ possible conformations, each of which incurs an energy penalty $\exp(-E_b/k_BT)$. Hence, the average $W_{2,2}$(b,s) for the SAW and for the NRRW is $[(z - 2)\exp(-E_b/k_BT)]/[z_{b1}(z - 2)] = \exp(-E_b/k_BT)/z_{b1}$.

The counting factors $N_{n+1,s}(\alpha,\beta)$ enumerate the number of pairs of united atom groups i and j in the whole polymer chain, such that the connecting path between i and j both traverses the local structure s and includes the pair of bonds α and β for all possible placements of the local structure within the chain. For example, consider $N_{2,1}$(b,b). Structure 1 of Figure 3a appears only along the backbone in PP, with the pair of bonds spanning separate but adjacent monomers. Therefore, $\rho_{PP} - 1$ equivalent sites contain this unique structure, where the polymerization index is $\rho_{PP} = (M - 1)/3$. The starting point i for a path traversing the kth appearance of unique structure 1 of Figure 3a in the PP chain can begin on any of the three united atom groups within the first through kth monomers. The end point j of the path cannot lie on the united atom group that is common to the two (b,b) bonds. Therefore, the summation over points j must omit that point, leaving all the monomers between the $(3k + 2)$nd united atom group and the end of the chain [the $(3r + 1)$st united atom group] as viable ending points j for the path. Hence, the total number $N_{2,1}$(b,b) of paths which include unique structure 1 of Figure 3a for a PP chain with polymerization index ρ_{PP} is

$$N_{2,1}(\mathrm{b,b}) = \sum_{k=1}^{\rho_{PP}-1}\sum_{i=1}^{3k}\sum_{j=3k+2}^{3\rho_{PP}+1} 1 = \frac{9\rho_{PP}(\rho_{PP} - 1)(\rho_{PP} + 1)}{6} \tag{A.2}$$

where the outer sum on k runs over all possible placements of the unique structure in the chain, while the sums on i and j run over all possible placements of the path from i to j that traverse this unique structure.

Similar calculations apply for $N_{2,2}$(b,b) and $N_{2,2}$(b,s). Since structure 2 of Figure 3a coincides with the structure of the propyl monomer, there are ρ_{PP} possibilities for placing this unique structure on the PP chain. The backbone−backbone pair on the kth monomer contributes to $N_{2,2}$(b,b) for paths beginning at any of the united atom groups on the $k - 1$ previous monomers. In addition, the first united atom group on the kth monomer can serve as a starting point for the path, while all united atom groups after the kth monomer can serve as the ending point for the path. This produces the formula for $N_{2,2}$(b,b) as

$$N_{2,2}(\mathrm{b,b}) = \sum_{k=1}^{\rho_{PP}}\sum_{i=1}^{3k-2}\sum_{j=3k+1}^{3\rho_{PP}+1} 1 = \frac{\rho r_{PP}(9\rho_{PP}^2 - 9\rho_{PP} + 6)}{6} \tag{A.3}$$

where the summation indices i, j, and k take the same significance as in eq A2.

The calculation of $N_{2,2}$(b,s) is more complicated, since either the beginning or the end of the path must contain

the side chain united atom group. If the path ends on the kth side chain, the sum over starting points is identical to the sum over i in eq A3, while if the path starts on the kth side chain, the sum over ending points is identical to the sum over j in eq A3. Adding these two contributions then yields $N_{2,2}$(b,s) as

$$N_{2,2}(\mathrm{b,s}) = \sum_{k=1}^{\rho_{pp}} \left(\sum_{i=1}^{3k-2} + \sum_{j=3k+1}^{3\rho_{pp}+1} \right) 1 = \rho_{pp}\,(3\rho_{pp} - 1) \quad \text{(A.4)}$$

Note that because the path either begins or ends on a side group, eq A4 contains only a double sum over the possible placements of the other end and of the unique structure within the chain.

All topological structures used in determining the configurational averaging for $W_{n+1,s}(\alpha,\beta)$ in the present work are depicted in Figure 3. The corresponding $N_{n+1,s}(\alpha,\beta)$ and $W_{n+1,s}(\alpha,\beta)$ are presented in Tables 1 and 2, with the index s matching the numbering in Figure 3 and with $n + 1$ denoting the number of bonds along the connecting path. The PE case is simplest because only the backbone−backbone pairs of bonds contribute nonzero $N_{n+1,s}(\alpha,\beta)$ of the general form

$$N_{n+1,1}(\mathrm{b,b}) = \frac{(\mathrm{M} - n - 1)(M - n)(M - n + 1)}{6} \quad \text{(A.5)}$$

The counting factors $\{N\}$ for the remaining branched structures are summarized in Table 1. Table 2 provides the averages $\{W\}$ for both the SAW and the NRRW models with connecting paths of up to four bonds. Note that the averages differ between the two walk models only for four or more bonds. The leading term Δ in eq 2.14 is simply the number N_1 of ways that all paths can pass through any individual bond, summed over all bonds in the chain. Δ is readily evaluated as $(M - 1)M(M + 1)/6$, $(M - 1)^2(M + 2)/9$, $(M - 2)[(M - 2)^2 + 12(M - 2) + 107)/12$, $(M - 1)[(M - 1)^2 + 27(M - 1) - 4]/12$, $(M - 1)[(M - 1)^2 + 6(M - 1) - 3]/9$ and $(M - 1)[4(M - 1)^2 + 15(M - 1) + 11]/30$, respectively, for the united atom PE, PP, P2B, PIB, hhPP, and PEP models of Figure 1.

References and Notes

(1) Cowie, J. M. G.; Nakata, S.; Adams, G. W. *Macromol. Symp.* **1996**, *112*, 207.
(2) Krishnamoorti, R.; Graessley, W. W.; Balsara, N. P.; Lohse, D. J. *Macromolecules* **1994**, *27*, 3073.
(3) Krishnamoorti, R.; Graessley, W. W.; Balsara, N. P.; Lohse, D. J. *J. Chem. Phys.* **1994**, *100*, 3894.
(4) Krishnamoorti, R.; Graessley, W. W.; Fetters, L. J.; Garner, R. T.; Lohse, D. J. *Macromolecules* **1995**, *28*, 1252.
(5) Graessley, W. W.; Krishnamoorti, R.; Reichart, G. C.; Balsara, N. P.; Fetters, L. J.; Lohse, D. J. *Macromolecules* **1995**, *28*, 1260.
(6) Balsara, N. P.; Fetters, L. J.; Hadjichristidis, N.; Lohse, D. J.; Han, C. C.; Graessley, W. W.; Krishnamoorti, R. *Macromolecules* **1992**, *25*, 6137.
(7) Walsh, D. J.; Graessley, W. W.; Datta, S.; Lohse, D. J.; Fetters, L. J. *Macromolecules* **1992**, *25*, 5236.
(8) Bates, F. S.; Schulz, M. F.; Rosedale, J. H.; Almdal, K. *Macromolecules* **1992**, *25*, 5547.
(9) Bates, F. S.; Fredrickson, G. H. *Macromolecules* **1994**, *27*, 1065.
(10) Fredrickson, G. H.; Liu, A. J.; Bates, F. S. *Macromolecules* **1994**, *27*, 2503.
(11) Fredrickson, G. H.; Liu, A. J. *J. Polym. Sci., Part B: Polym. Phys.* **1995**, *33*, 1203.
(12) Gehlsen, M. D.; Bates, F. S. *Macromolecules* **1994**, *27*, 3611.
(13) Singh, C.; Schweizer, K. S. *Macromolecules* **1995**, *28*, 8692. Earlier discusion of the competition between stiffness and enthalpic interactions are given in: Schweizer, K. S. *Macromolecules* **1993**, *26*, 6050.
(14) Singh, C.; Schweizer, K. S. *J. Chem. Phys.* **1995**, *103*, 5814; **1997**, *30*, 1490.
(15) Weinhold, J. D.; Kumar, S. K.; Singh, C.; Schweizer, K. S. *J. Chem. Phys.* **1995**, *103*, 9460.
(16) (a) Schweizer, K. S.; David, E. F.; Singh, C.; Curro, J. G.; Rajasekaran, J. J. *Macromolecules* **1995**, *28*, 1528. (b) Rajasekaran, J. J.; Curro, J. G.; Honeycutt, J. D. *Macromolecules* **1995**, *28*, 6843.
(17) Schweizer, K. S.; Singh, C. *Macromolecules* **1995**, *28*, 2063.
(18) Dudowicz, J.; Freed, K. F. *Macromolecules* **1996**, *29*, 8960.
(19) Freed, K. F.; Dudowicz, J. *Macromolecules* **1996**, *29*, 625.
(20) Foreman, K. W.; Freed, K. F., *J. Chem. Phys.* **1997**, *106*, 4067.
(21) Foreman, K. W.; Freed, K. F. (a) *Adv. Chem. Phys.*, in press; (b) Foreman, K. W.; Freed, K. F.; Ngola, I. M. *J. Chem. Phys.* **1997**, *107*, 4688.
(22) Bawendi, M. G.; Freed, K. F. *J. Chem. Phys.* **1987**, *86*, 3720.
(23) Madden, W. G.; Pesci, A. I.; Freed, K. F. *Macromolecules* **1990**, *23*, 1181.
(24) Dudowicz, J.; Freed, K. F. *Macromolecules* **1991**, *24*, 5076.
(25) Binder, K.; Heermann, D. W. *Monte Carlo Simulations in Statistical Physics: An Introduction*; Springer: Berlin, 1988.
(26) Baumgartner, A. In *Applications of the Monte Carlo Methods in Statistical Physics*; Binder, K., Ed.; Springer: Berlin, 1984; Chapter 5.
(27) Zimm, B. H.; Stockmayer, W. H. *J. Chem. Phys.* **1949**, *17*, 1301.
(28) Yamakawa, H. *Modern Theory of Polymer Solutions*; Harper & Row: New York, 1971.
(29) Flory, P. J. *Proc. R. Soc. London, Ser. A* **1956**, *234*, 60.
(30) Nemirovsky, A. M.; Dudowicz, J.; Freed, K. F. *Phys. Rev. A* **1992**, *45*, 7111.
(31) Jinnai, H.; Hasegawa, H.; Hashimoto, T.; Han, C. C. *Macromolecules* **1992**, *25*, 6078.
(32) Hayashi, H.; Flory, P. J.; Wignall, G. D. *Macromolecules* **1983**, *16*, 1328.
(33) Krishnamoorti, R.; Graessley, W. W.; Dee, G. T.; Walsh, D. J.; Fetters, L. J.; Lohse, D. J. *Macromolecules* **1996**, *29*, 367.
(34) Dudowicz, J.; Freed, K. F. *Macromolecules* **1995**, *28*, 6625.
(35) Dudowicz, J.; Freed, K. F. *Macromolecules* **1990**, *23*, 1519.
(36) Dudowicz, J.; Freed, K. F. *J. Chem. Phys.* **1992**, *96*, 9147.

MA970337U